NANOPARTICLE-FACILITATED TRANSPORT OF PHOSPHORUS IN POULTRY-LITTER AMENDED GRASSLAND

by

RUSSELL DEAN HENDERSON

(Under the Direction of Aaron Thompson)

ABSTRACT

Managing P loss from poultry litter amended pastures has regional importance to the health of sensitive ecosystems. Typical sampling methodology considers that which passes through a 0.45 μm filter as “dissolved” P but many P sorbing particles that behave differently than truly dissolved aquo-ions are <0.45 μm and this misclassification may cause errors in predictive models. We assessed the contribution of colloid and nanoparticle-bound P (nPP; 1 nm – 415 nm) to P released from these soils after oxic, anoxic, and pH adjusted laboratory incubations and to runoff P in fescue watersheds that typically received bi-annual poultry litter applications since 1995. Soil incubations indicated anoxic conditions in seasonally saturated fields were potentially a major source of generating nPP in solution. An average of 10% of <0.415 μm runoff P was present as nPP. Understanding conditions responsible for P loss in agricultural systems and the forms of this P may lead to preventing such loss.

INDEX WORDS: phosphorus, poultry litter, nanoparticles, runoff, anoxic

NANOPARTICLE-FACILITATED TRANSPORT OF PHOSPHORUS IN POULTRY-LITTER AMENDED GRASSLAND

by

RUSSELL DEAN HENDERSON

B.S. Clemson University, 2008

A Thesis Submitted to the Graduate Faculty of The University of Georgia in Partial Fulfillment of the Requirements for the Degree

MASTER OF SCIENCE

ATHENS, GEORGIA

2011

NANOPARTICLE-FACILITATED TRANSPORT OF PHOSPHORUS IN POULTRY-LITTER AMENDED GRASSLAND

by

RUSSELL DEAN HENDERSON

Major Professor:	Aaron Thompson
Committee:	Miguel Cabrera William Miller

Electronic Version Approved:

Maureen Grasso
Dean of the Graduate School
The University of Georgia
May 2011

ACKNOWLEDGEMENTS

I thank Vaughn Calvert, Frank Newsome, and John Rema for logistical and sampling assistance in the field and Gene Weeks for ICP-MS analysis. I am indebted to the long term field and project support of the Central Georgia Research and Education Center. Funding was provided by the United States Department of Agriculture (USDA), AFRI (Grant # 2009-65107-05830) and the University of Georgia Research Foundation (Grant # FRG 767).

TABLE OF CONTENTS

Page

CHAPTER

APPENDICES

LIST OF TABLES

Page

LIST OF FIGURES

CHAPTER 1

INTRODUCTION

The effects of agricultural management practices on runoff volume, quality, and phosphorus (P) losses have been studied in depth (Butler et al., 2008; Franklin et al., 2006; Franklin et al., 2007; Kuykendall et al., 1999). This is especially true in cases where broiler litter is surface applied as a fertilizer because the potential for P loss is increased (Butler et al., 2008; Franklin et al., 2006; Franklin et al., 2007). Preventing P transport to surface waters remains a central concern in mitigating the harmful effects of eutrophication on exposed water bodies. Traditionally, mobilized P has been separated into “particulate-P” and “dissolved-P” via filtration through 0.45 μm (Haygarth and Sharpley, 2000). However, particles < 0.45 μm present some of the most abundant and reactive surfaces in soil and environmental systems (Hochella et al., 2008; Kretzschmar et al., 1999) due to their high surface areas ($>10\ m^2\ g^{-1}$) and the high binding efficiency of metal-oxide or organic surface functional groups which are typically present. They can be potent carriers of metals, carbon, and nutrients—facilitating longer transport distances than would be predicted for dissolved ions (de Jonge et al., 2004; Heathwaite et al., 2005; Makris et al., 2006). Indeed, P strongly binds to high-surface area Fe and Al-bearing nanoparticles and organic matter, all of which have been implicated in P transport in river systems (Lin et al., 2009; Mayer and Jarrell, 1995; Olli et al., 2009).

The two major forms of soil P are soluble orthophosphate and fixed mineral P. Orthophosphate (PO_4) exists in three predominant forms based on the degree of protonation,

$H_2PO_4^{1-}$, HPO_4^{2-}, and PO_4^{3-}, with pKa values of 2.15, 6.86 and 12.32, respectively. Fixed mineral P is comprised of P either a) bound to Fe, Al, or Mn (oxy)hydroxides which predominates in acidic soils and are insoluble at pH 4 to 7, or b) tied up in Ca or Mg minerals which predominate in basic soils and are insoluble at pH >7. The conversion of fixed mineral P to soluble orthophosphate is governed by the interaction of pH and redox potential. Redox processes, as brought on by reducing conditions, dissolve the compounds bonded to P. Reduction occurs when a soil becomes saturated and molecular oxygen is consumed (Vepraskas and Faulkner, 2001). This reduction process can desorb P bound to Fe(III) and Mn(IV) into the soil solution (Ann et al., 2000). These reductions also result in the production of hydroxide ions thereby increasing the soil solution pH (Thompson et al., 2006).

$$Fe^{III}(OH)_3(s) + e^- \rightarrow Fe^{2+}(aq) + 3\ OH^-(aq) \qquad \text{(Equation 1)}$$

The site we chose to study P release and transport has received broiler litter amendments bi-annually for 12 of the last 15 years and has known areas that are and are not seasonally saturated. These conditions have allowed for the accumulation of P in these soils over time. Our study objectives are (i) to evaluate how soil redox and pH influence the release of these nanoparticles, (ii) to determine the contribution of nanoparticle-bound P (nPP) to released Molybdate-reactive P (MRP) in pasture runoff water, and (iii) to characterize the size and composition of these nanoparticles. We hypothesized (i) that low redox conditions would increase nanoparticle dispersion and (ii) nPP to be a significant portion of MRP loss in runoff. Our results indicate that P released from the soils of these grasslands after subjugation to anoxic conditions was ~80 ± 10% nPP, with the highest measurements of nPP and total P occurring in soils that are seasonally saturated. We also found that nPP comprises up to 21% of the <0.415 μm MRP in runoff from grasslands. The nanoparticles released from the soils during anoxic incubations resembled those in the runoff and our data suggest nPP is predominately associated with 1 – 3 nm metal-oxide nano-particles imbedded in mineral aggregates averaging 200 – 300 nm in diameter. These aggregates are composed of flakes of layered silicates (most likely kaolinite), Fe, Al, and Ti rich oxides, and possibly organic matter.

CHAPTER 2

LITERATURE REVIEW

Nanoparticles in the Environment

Nanoparticles are size-defined entities having at least one dimension between 1 nm and 1 μm. They often have high specific areas (e.g. >10 m^2 g^{-1}) making them important sorbents for nutrients and contaminants. In the surfaces of fresh waters, they can occur as products of soil weathering, Fe(III) and Mn(III,IV) oxides, biological debris, humus colloids, and colloidal Fe(OOH) oxides stabilized by humic or fulvic acids (Kretzschmar et al., 1999). Many studies have been conducted in the last two decades to characterize nanoparticles found in agricultural systems and surface waters and to quantify the capacity of these nanoparticles to transport nutrients, especially phosphorus (P). For instance, Haygarth et al. (1997) found that in leachate from a grassland, truly dissolved P that was <1000 Da (≈ 1 nanometer) accounted for 87% of the total reactive P present. In soil-water extracts from a grassland and an arable field, Hens and Merckx (2002) found 40 – 58% of < 0.45 μm molybdate reactive P (MRP) was bound to particles 0.025 μm – 0.45 μm. After simulated rainfall on undisturbed soil columns of an agricultural field, de Jonge et al. (2004) found that ~75% of the P found in the resulting leachate was bound to nanoparticles <0.24 μm. Haygarth et al. (1997) also showed that in soil surface runoff samples as much as 86% of total reactive P did not pass through a 1000 Da ultrafilter and 71% of total reactive P did not pass through a 0.45 μm filter. Additionally, in surface waters from two rivers, they showed <1000 Da P only accounted for 55% of the total reactive P. Turner et al. (2004) have shown as much as 56% of P in surface runoff was bound to particles in the 1 nm – 1 μm size range. Similarly, in fresh water surfaces, Filella et al. (2006) have shown up to 26% ± 6% of P fell within the 3000 Da – 1.2 μm range.

Nanoparticles can be generated by physical fragmentation and erosion of existing solid phases and by the precipitation and nucleation of ions from solution. Likewise, a host of processes act to remove nanoparticles from solution, including particle coagulation, attachment and settling, and dissolution. Large reductions in free energy can be realized through particle agglomeration and thus nanoparticles readily coagulate and form nano or micro-scale aggregates. Nanoparticle stability is affected by adsorbates that alter their surface charge and by interparticle attractive and repulsive forces (Stumm and Morgan, 1996).

Changes in soil solution chemistry are the most common cause for the release of nanoparticles in soil and groundwater. Because the diffusive forces associated with Brownian motion of suspended nanoparticles are greater than the sedimentation rate, nanoparticles remaining stable in suspension over extended periods of time. The stability time of nanoparticles can range from fractions of a second to years and is a balance of attractive and repulsive forces. If attractive forces are greater than repulsive forces, nanoparticles coagulate and settle out of suspension. If the inverse is true, nanoparticles are repelled from each other and remain dispersed in suspension. The coagulation state of nanoparticles is important because they are major sorbents for nutrients and contaminants. If coagulated, they are less likely to be lost to leaching. If dispersed, they can leach or clog pores in soil. Since soil solution chemistry affects the surface chemistry of nanoparticles, understanding the chemical processes occurring in a soil system will improve the understanding of the coagulation state of nanoparticles in the soil system (Kretzschmar et al., 1999).

Surface Charge of Nanoparticles

The surface charge of nanoparticles influences the manner in which they flocculate and coagulate. The five components of surface charge in soils are: net structural surface charge density (σ_0), inner-sphere complex surface charge density (σ_{IS}), outer-sphere complex surface charge density (σ_{OS}), net proton surface charge density (σ_H), and diffuse layer surface charge density (σ_d); The sources of these five components are: isomorphic substitutions, inner-sphere surface complexes of ions, outer-sphere complexes of ions, H^+/OH^- surface complexation, and diffuse layer adsorption of ions respectively.

Surfaces of solid particles in soils can develop electrical charge either permanently from isomorphic substitutions of component ions in the bulk structure of a solid or conditionally from reactions of surface functional groups on a solid with adsorptive ions in solution. This electrical charge is expressed in moles of charge per kilogram.

Permanent structural charge (σ_0) is a result of isomorphic substitution. Primary and secondary minerals undergo isomorphic substitution but this process only produces a significant surface charge in 2:1 layer silicates. Permanent structural charge for layered silicates is defined as:

$$\sigma_0 = -(x / M_r) \cdot 10^3 \qquad \text{(Equation 2)}$$

where x is the layer charge and M_r is molecular mass.

Net proton surface charge density is proportional to the difference between the moles of protons and the moles of hydroxide ions compounded by surface functional groups:

$$\sigma_H = q_H - q_{OH} \qquad \text{(Equation 3)}$$

where q_H is moles of H^+ and q_{OH} is moles of OH^-. It does not theoretically include diffuse layer protons. The value of σ_H can be positive, zero, or negative based on pH and ionic strength (Sposito, 2000).

The intrinsic surface charge (σ_{in}) of a soil is defined as:

$$\sigma_{in} = \sigma_0 + \sigma_H \qquad \text{(Equation 4)}$$

The amount of weathering upon the minerals and organic matter of a soil will determine the contribution of σ_0 and σ_H to σ_{in}. The siloxane cavity is the leading surface site expression of permanent charge and is found in soils at the early and intermediate stages of weathering. These soils are often referred to as permanent-charge soils because σ_0 is the primary contributor to the intrinsic surface charge (σ_{in}). In soils at the advanced stage of weathering, there are numerous minerals bearing reactive OH groups. These soils are referred to as variable-charge soils because σ_H is the main source of σ_{in}. Changes in pH play a major role in the development of surface charge in variable-charged soils.

The total net particle charge (σ_P) is defined as:

$$\sigma_p = \sigma_0 + \sigma_H + \sigma_{IS} + \sigma_{OS} \qquad \text{(Equation 5)}$$

This value can be positive, zero, or negative and is a function of the soil solution composition.

Particles must always be electrically neutral. When the net proton surface charge density, inner-sphere surface charge density, and the outer-sphere surface charge density do not equal zero, then the diffuse layer surface charge density must balance the net total surface charge. The diffuse layer consists of ions that are not bound into surface complexes in the soil solution but are still adsorbed by soil particles. The ions move freely in the soil solution but are close enough to solid surfaces to balance the net total particle surface charge, thus:

$$\sigma_p + \sigma_D = 0 \qquad \text{(Equation 6)}$$

Points of Zero Charge

Points of zero charge are pH values where one or more of the surface charge components disappear at a fixed temperature, applied pressure, and aqueous solution composition. At the point of zero charge (PZC), no σ_P exists for neutralization by ions in the diffuse layer and thus all adsorbed ions are immobilized in surface complexes: $\sigma_P = 0$. The PZC can be measured by determining the pH value where soil particles are unresponsive to an applied electrical field. This determines the pH value where the particle electrophoretic mobility disappears and is known as the isoelectric point. Another way to measure the PZC is to determine the pH value where charge balance exists in an aqueous solution with suspended particles. The PZC indicates the lack of freely moving adsorbed ions and the increase of interparticle forces that cause coagulation. Coagulation is at maximum in variable charge systems when pH = PZC. The result is that the PZC is important in particle aggregate formation and it reduces the potential for particulate loss through leaching in variable-charged soils. These soils typically weather to pH values around their PZC. This being stated, in the event that pH = PZC:

$$\sigma_H = -(\sigma_0 + \sigma_{IS} + \sigma_{OS}) \qquad \text{(Equation 7)}$$

Based on this equation and given that σ_H is inversely varied with pH, the pH must increase with the increase of $\sigma_{IS} + \sigma_{OS}$ and decrease with the decrease of $\sigma_{IS} + \sigma_{OS}$. For example, if σ_{IS} increases by additional K^+ ion adsorption, then σ_H at the PZC will decrease and the PZC will increase. In general, surface complex formation moves the PZC in the same manner as the change in net surface complex charge. The adsorption of cations in surface complexes will raise the PZC whereas anions will lower it.

At the point of zero net proton charge (PZNPC) σ_H disappears: $\sigma_H = 0$. In the event that pH = PZNPC:

$$\sigma_0 = -(q_+ - q_-) \qquad \text{(Equation 8)}$$

where q_+ is moles of adsorbed cations and q_- is moles of adsorbed anions. Based on this equation, adsorbed ions, other than H^+ or OH^- in σ_H, balance permanent structural charge when pH = PZNC. This allows for σ_0 to be determined by adjusting the pH to the PZNPC and measuring the net adsorbed ion charge (Sposito, 1992).

At the point of zero net charge (PZNC), σ_{in} disappears: $\sigma_{in} = \sigma_{IS} + \sigma_{OS} + \sigma_D = 0$. The PZNC is determined by saturating a soil with know concentrations of Na^+ and Cl^- and adjusting the pH to the point where $q_{Na} = q_{Cl}$. In the event that pH = PZNC:

$$q_+ - q_- \equiv \sigma_{IS} + \sigma_{OS} + \sigma_D = 0 \qquad \text{(Equation 9)}$$

Mobile ions are present at the PZNC but not for the PZC. This could have major implications for nutrient and contaminant retention in soils (Sposito, 2000).

Sorption Processes of Phosphorous and Effects of Anoxia

The three major forms of soil P are organic P, fixed mineral P, and orthophosphate (Vepraskas and Faulkner, 2001). The reactivity and solubility of these forms of P are actuated by the chemical, physical, and biological characteristics of the system. Redox potential, pH, temperature, microbial activity, and soluble P concentrations also influences P solubility (Ann et al., 2000). Phosphorus adsorption occurs through both weak bonding forces, such as van der Waals forces and electrostatic outer-sphere complexes, as well as strong bonding interactions, such as inner-sphere complexes with higher covalent bond character (Scheidegger and Sparks, 1996). The valence of P in soil is constant at +5 and thus P is not directly affected by redox processes. However, P solubility in water and soil is affected by redox processes that decompose and dissolve compounds bonded to P (Vepraskas and Faulkner, 2001).

The interaction of redox potential and pH governs the conversion of fixed mineral P into soluble orthophosphate. Orthophosphate sorption to Fe and Al oxides and hydroxides is maximized at pHs between 4 and 7. The dissolution rate of Al and Fe oxides and hydroxides increases substantially below pH 4 and releases bound orthophosphates. The valence of Al in soil is constant and thus Al is unaffected by redox potential. The main conversions at pHs greater than 7 are precipitation as insoluble Ca- or Mg-phosphates or adsorption to carbonates. Ca and Mg do not undergo redox reactions and thus solubility of Ca- and Mg-phosphates is primarily dictated by pH (Vepraskas and Faulkner, 2001).

Phosphorus is held by Fe(III), Mn(IV), and Al-minerals in noncalcareous soils during oxic conditions. When extended flooding and reducing conditions prevail in a soil system, a state of anoxia is induced in which dissolved reactive P is desorbed to the surrounding water. This desorption occurs when Fe(III) and Mn(IV) phases with co-precipitated or surface bound P are microbially reduced to the highly soluble Fe(II) and Mn(II) (Ann et al., 2000).

The amount of oxalate-extractable Al and Fe(III) oxides and hydroxides in a soil directly affects how much P the soil can adsorb. The formation of amorphous Fe(II) hydroxides during flooding and reducing conditions of an oxidized soil may increase the P sorption of the soil. Amorphous Fe(II) hydroxides have larger surface areas and thus a greater number of sorption sites than Fe(III) oxides that are more crystalline. Once P sorption exceeds the number of sites, any remaining P can be rapidly removed with the bulk water (Vepraskas and Faulkner, 2001).

Anoxic conditions hinder the decomposition of organic matter, causing it to accrue in the soil. Organic ions compete for binding sites with phosphate ions and reduce the inorganic P sorption capacity of the soil. However, organic matter can hinder the crystallization of Al and Fe oxides leading to an enrichment in short-range-ordered Al- and Fe-hydroxide minerals. These minerals increase the inorganic P sorption capacity of the soil (Darke and Walbridge, 2000). Additionally, organic matter itself greatly contributes to P sorption capacity of a system, particularly in a system subjected to prolonged anoxic conditions. Increased reduction decreases soil total P by dissolution of P sorbing minerals (Miller et al., 2001). Understanding these various sorption processes of P is essential to developing management practices that reduce the loss of P from agricultural systems. Given all that is known about P sorption and release in soil, more research is needed to better understand the field conditions that contribute to P release, to quantify the amount of P released under these conditions, and to characterize the forms of P released in given agricultural systems.

CHAPTER 3

ANOXIA-INDUCED RELEASE OF COLLOID AND NANOPARTICLE-BOUND PHOSPHORUS IN POULTY-LITTER AMENDED GRASSLAND[1]

---

[1] Henderson, Russell D., N. Mantripragada, N. Kabengi, M. Cabrera, S. Hassan, A. Thompson, To be Submitted to the Soil Science Society of America Journal

Abstract

High rainfall and seasonal soil saturation in the Georgia Piedmont generate conditions where soil colloids and nanoparticles could be mobilized. In soils with high P concentrations due to poultry litter applications, these mobilized particles may contain significant P. Thus understanding the conditions governing particle mobilization is an essential component in reducing P loss from these soils. We assessed contributions of colloid and nanoparticle-bound P (nPP; 1 nm – 415 nm) to P released from field surface soils of six 0.8-ha fescue grasslands that had received bi-annual poultry litter applications since 1995. In laboratory incubations, the soils were equilibrated at pH 6 and 8 and subjected to 7 d of anoxic conditions. Samples were size fractionated by differential centrifugation and ultrafiltration and analyzed for total P, Al, Fe, Si, Ti, and Ca , as well as Molybdate-reactive P (MRP). Selected samples were visualized via transmission electron microscopy (TEM) and energy dispersive X-ray spectroscopy (EDS). In the soil incubation solution, we found released nanoparticles that had a mean diameter of 250 nm and were composed of aggregates of ~50 nm aluminosilicate flakes with clusters of <10 nm Fe and Ti-rich phases which contained most of the P detected by EDS. The release of nPP following anoxic incubation was substantial in soils collected from seasonally saturated fields, while minimal in soils from well-drained fields. This corresponded with greater Fe^{2+}(aq) production during incubation in the seasonally saturated soils. Non-reductive particle dispersion initiated through the addition of base did not result in nPP release. This suggests Fe is acting as a cementing agent binding P-baring colloids to the bulk soil, which can be readily released upon onset of reducing conditions. Furthermore, it suggests soils that are periodically exposed to anoxic conditions may be more susceptible to redox-induced P mobilization.

Introduction

Much effort has been put forth to analyze the effects of agricultural management practices on P movement in and from fields (Butler et al., 2008; Franklin et al., 2006; Franklin et al., 2007; Kuykendall et al., 1999). The need for this is particularly essential in systems where broiler litter is surface applied as a fertilizer since this practice increases the potential for P loss. Thus, many have worked to evaluate the mechanisms of P loss and develop ways to lessen P loss following broiler litter amendments (Butler et al., 2008; Franklin et al., 2006; Franklin et al., 2007). Standard methods for measuring P in soil solutions involve deeming that which passes through a 0.45 um filter as “dissolved-P” (Haygarth and Sharpley, 2000). However, this may underestimate “particulate-P” as potential P binding particles < 0.45 μm may be present. These particles are among the most abundant and reactive surfaces in a soil solution (Hochella et al., 2008; Kretzschmar et al., 1999) given their high surface areas ($>10\ m^2\ g^{-1}$) and the high binding efficiency that results from their typical composition of metal-oxide and/or organic matter. They also travel further than dissolved ions, taking bound nutrients, metals, and contaminants greater distances than expected for their unbound forms (de Jonge et al., 2004; Heathwaite et al., 2005; Makris et al., 2006).

The strong binding of P to colloids and nanoparticles has been implicated in P transport in soil solutions. In leachate from undisturbed soil columns of an agricultural field, de Jonge et al. (2004) showed that nanoparticles <0.24 μm transported around 75% of the P leached. In leachate from grasslands Haygarth et al. (1997) showed that the >1000 Da fraction constituted 13% of total reactive P present. In soil-water extracts from a sandy grassland and sandy arable field Hens and Merckx (2002) showed particles ranging from 0.025 μm – 0.45 μm comprised 40 – 58% of < 0.45 μm MRP present.

There currently is a need to better understand what factors contribute to the release of soil colloids and nanoparticles for a given system. It is known that changes in pH, Eh, soil solution chemistry, and decreases in ionic strength can release these particles (Chorover and Sposito, 1995; Pokrovsky and Schott, 2002; Itami and Fujitani, 2005; Ryan and Gschwend, 1994; Thompson et al., 2006). Ryan and Gschwend (1994) showed that nanoparticles can be mobilized by increasing electrostatic repulsion between nanoparticle surfaces in samples from an Atlantic Coastal Plain aquifer of New Jersey. Concurrently, Thompson et al. (2006) showed that the dynamics of nanoparticles were dependent on pH changes that accompanied redox oscillations in samples from a basaltic upland forest soil of Maui, Hawaii. Also Pedrot et al. (2009) and Grybos et al. (2007) showed that mobilization of trace elements typically bound to organic nanoparticles was due to increased pH in wetland soils of Brittany, Western France. However, Rick and Arai (2011) found that nanoparticles 10-200 nm did not significantly contribute to P transport in Ultisols from South Carolina agricultural fields containing excessive P before and after these soils underwent significant pH increases. In light of this, other soil processes should be studied to determine what if any other factors may contribute to P bearing colloid and nanoparticle release in these soils. Additionally, as Rick and Arai (2011) suggested, the composition of released particles should be analyzed as their type may dictate whether or not they are reactive with P.

In our study we selected a site in the Georgia Piedmont with high P loading from bi-annual broiler litter applications for 12 of the last 15 years and that contains fields that are and are not seasonally saturated to study P release and transport. Thus, our study objectives are (i) to evaluate how soil redox and pH influence the release of these nanoparticles and (ii) to characterize the size and composition of these nanoparticles. We hypothesized that low redox conditions would increase nanoparticle dispersion.

Materials and Methods

For our assessment of nanoparticle-bound P (nPP), we selected a well-instrumented poultry litter amended grassland at the Central Georgia Research and Education Center in Eatonton, GA that contains P in excess and has shown considerable losses of dissolved reactive P during runoff events (Franklin et al., 2006; Franklin et al., 2007; Kuykendall et al., 1999; Pierson et al., 2001). Soil samples were subjected to multiple, operationally defined incubations. Nanoparticles from soil incubations were size fractionated using a combination of differential centrifugation and ultrafiltration. Nanoparticle characterization was carried out by inductively coupled plasma-mass spectrometry (ICP-MS) and transmission electron microscopy (TEM).

We collected surface soil samples following a litter application (Nov. 2009) from six 0.8-ha, fescue/bermudagrass hay fields with similar soil classifications (Typic Kanhapludults, Aquic Hapludults, and Aquultic Hapludalfs), similar topsoil (sandy loam), and similar depth of topsoil at the Central Research and Education Center (Eatonton, Georgia). Fields 1, 2, 3, and 6 have had poultry litter applied at a rate of 2.5 Mg litter ha^{-1} bi-annually since 1995 with the exception of 1997 through 1999 (Figure 3.1). Fields 2 and 6 have been aerated immediately following litter application since 2000. From 2000 to 2002 aeration was preformed with an AerWay 80Q to a depth of 10 to 12 cm. From 2002 to the present aeration was preformed with a custom-made machine bearing ammonia knives to a depth of 9 cm. These aerated fields are paired with nonaerated fields 1 and 3 respectively as these pairings maximize consistency between soil type and soil hydrology. Fields 1 and 2 are considered well-drained fields and Fields 3 and 6 are considered somewhat poorly-drained fields. Fields 7 and 9 are control fields managed similarly without any application of litter (Franklin et al., 2007). Soil sampling was conducted 18 d after poultry litter application. Twenty samples were taken from each field with a push probe to a depth of 5 cm and mixed to generate a composite soil sample for each field. The composite samples were transported to the laboratory where they were stored at 4°C, in the dark (Thompson et al., 2005).

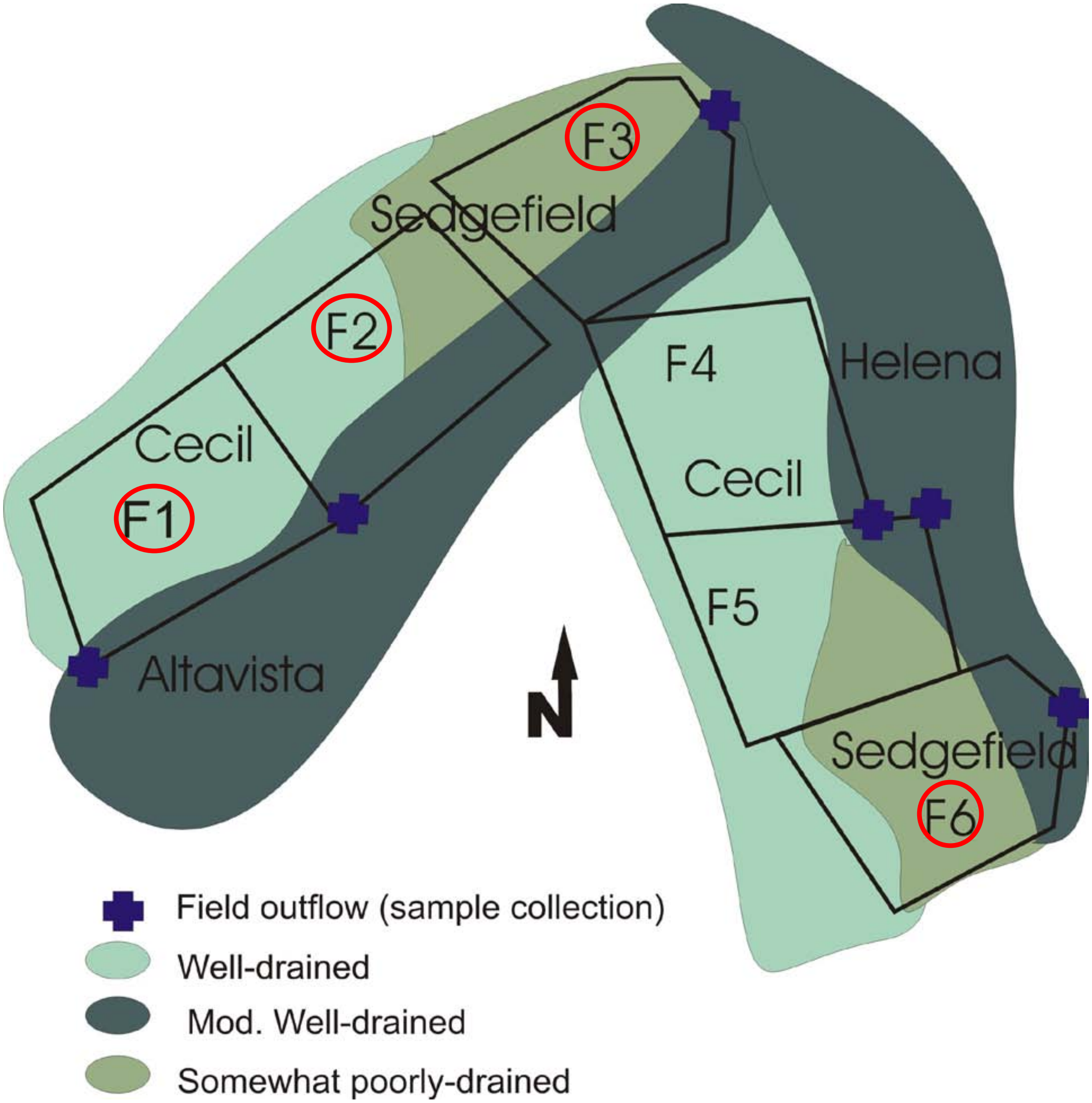

Figure 3.1. Soil series map and drainage classes for fields receiving poultry litter. Present soil series are: Altavista (fine-loamy, mixed, semiactive, thermic Aquic Hapludults), Cecil (fine, kaolinitic, thermic Typic Kanhapludults), Helena (fine, mixed, semiactive, thermic Aquic Hapludults), and Sedgefield (fine, mixed, active, thermic, Aquultic Hapludalfs) (Franklin et al., 2007). Red circles highlight fields used in soil incubations. Fields 1 & 2 are a considered well-drained and Fields 3 & 6 considered somewhat poorly-drained.

Soil samples from Fields 1, 2, 3, 6, 7, and 9 were prepared in triplicate for each of three incubations, operationally defined as Anoxic, Oxic, and Oxic KOH, in 16-mL Oak Ridge centrifuge tubes with 1:10 soil:solution (1.2 g of soil (dry weight equivalent):10.8 mL of 2.0 mmol KCl) and with sodium (Na) lactate (10 mM C L^{-1}) added as a carbon (C) source. The Anoxic incubation was conducted inside of a 95%:5% N_2:H_2 glovebox (Coy Vinyl Anaerobic Chambers, Grass Lake, MI) where samples were set on an end-over-end shaker (Thermo Scientific Labquake) at 8 rpm for 7 d. The Oxic incubation was shaken for 1 h at 280 rpm (Eberbach Reciprocal Shaker 6010). The Oxic KOH incubation had potassium hydroxide (KOH) added to increase the pH to approximately 8 before being shaken as described for the Oxic incubation. All reported pH values are those at the end of the equilibration period.

Supernatant from soil incubations was divided into four, 2-mL subsamples and placed in 2-mL centrifuge tubes for particle size-fractionation using a combination of differential centrifugation (Eppendorf Centrifuge 5430) and ultrafiltration to achieve estimated particle class separations of <415 nm, <260 nm, <35 nm, and <3Kda based on an assumed particle density of 2.4 g cm^{-3} (see Appendix A for Stokes-law calculations). The <415 nm particle class was obtained by spinning the samples at 1,088 rcf for 3 min. A 1-mL subsample of the supernatant was acidified to pH 3 with 0.1 M HCl for suspended elemental analysis and a 0.5-mL subsample of the supernatant was collected and stored, unacidified at 4°C for transmission electron microscopy (TEM) nanoparticle characterization (see section 2.6 below). The <260 nm and <35 nm particle classes were isolated by spinning the samples at 3,097 rcf for 3 min and 20,521 rcf for 24 min respectively; 1-mL subsamples of the supernatant were acidified as described above for elemental analysis. The <3 kDa particle class fraction was separated by first spinning samples as described for the <35 nm particle class and then passing 0.5 mL of the supernatant through a 3 kDa filter (Millipore Amicon$^{®}$ Ultra) at 20,817 rcf for 10 min, followed by acidification to pH 3. In all cases, we avoided floating leaf litter and debris by extracting the supernatants via pipette from below the surface layer.

We employed the method of differential centrifugation based on calculation of a stokes-effective particle size assuming spherical particles (Poppe et al., 1988). While this method avoids issues related to pore clogging associated with classical filtration through a membrane, it nevertheless introduces its own set of interpretive biases that need to be carefully considered during data analysis. Most importantly, because the technique relies on achieving differential particle separation through sedimentation calculated for a single mean particle density, individual particle densities that deviate from this nominal value will have different sedimentation rates, resulting in the removal of smaller particles with higher density and retention in the supernatant of larger particles of lower density. Predominately organic particles will have a much lower density than mineral-based particles and thus will be preferentially retained in the supernatant. For this reason, when using such a technique, it is always necessary to confirm particle size, geometry and composition with another independent analysis. In our case, we rely on TEM analyses.

We determined molybdate-reactive phosphorus (MRP) on all subsamples via the molybdate blue method (Murphy and Riley, 1962) with ultraviolet detection on a Shimadzu UV-1700 UV-Visible Spectrophotometer using a method detection limit of 0.4 ppm. The <415 nm and <3kDa separates of the soil incubations were also analyzed for total P, Al, Fe, Si, Ti and Ca on a Perkin Elmer-Sciex 9000 ICP-MS.

Transmission electron microscopy characterization was carried out on unacidified <415 nm subsamples from selected soil incubation samples. Dispersed nanoparticles from Field 2 and

6 were selected because these fields exhibited distinctly different drainage characteristics (seasonally wet vs. well-drained). Soil incubation samples were dialyzed (1 kDA, Spectrapor) against 1.7 x 10^5 Ω-m water to remove dissolved salts and the electrical conductivity was reduced from ~2250 μS m^{-1} to 1.25 μS m^{-1}. Samples were prepared by depositing one to three drops of the samples on a copper specimen grid coated with an ultrathin layer of carbon (Ted Pella, Inc.) and allowing the water to evaporate in a laminar flow hood. Images were obtained using a JEOL 2010F Transmission Electron Microscope operating at 200 kV (JEOL Ltd, Tokyo Japan). Information on the sample elemental compositions was collected using energy dispersive X-ray spectroscopy (Oxford detector).

Results

The majority of P released during the Oxic and Oxic KOH incubations, ~ 95 and ~84% respectively, passed through the 3 kDa filters whereas only ~25% of P released during the Anoxic incubation passed through these filters. Our data indicate <415 nm MRP (Figure 3.2) and total P (Figure 3.3) release was highest following the Oxic incubation for Fields 1 and 2 (well-drained) while Fields 3 and 6 (poorly-drained) released more P following the Anoxic incubation. However, for all fields, the greatest nanoparticle-bound total P release was due to the Anoxic incubation with 0.23 ± 0.01 mmol P Kg^{-1}, 0.45 ± 0.22 mmol P Kg^{-1}, 1.18 ± 0.36 mmol P Kg^{-1}, and 1.15 ± 0.13 mmol P Kg^{-1} observed for Fields 1, 2, 3, and 6 respectively. These values constituted 91 ± 3.6%, 88 ± 8.4%, 71 ± 23%, and 73 ± 1.4% (Figure 3.3) of the <415 nm total P released in fields 1, 2, 3, and 6 respectively. In contrast, the average released nanoparticle-bound total P observed for the Oxic and Oxic KOH incubations was notably less overall at 0.05 ± 0.04 mmol P $Kg^{-1}$and 0.14 ± 0.05 mmol P Kg^{-1} respectively for all fields. Across all fields and treatments, Mo reactive nPP was most plentiful, while highly variable, in the 3kDa – 35 nm particle size fraction. In fact, average Mo reactive nPP seemed to lessen as a function of increasing particle size with averages across all samples of 0.21 ± 0.33 mmol P kg^{-1}, 0.04 ± 0.04 mmol P kg^{-1}, and 0.02 ± 0.03 mmol P kg^{-1} for the 3kDa – 35 nm, 35nm – 260 nm, and 260 nm – 415 nm particle size fractions, respectively. Additionally, analysis of total P for these replications indicates much of the nPP is molybdate reactive (Figure 3.4).

We assessed the molar abundance of nanoparticle Fe, Si, Al (Figure 3.5), Ti, and Ca where we found Fe, Si, and Al concentrations to be within an order of magnitude of each other. There was no definitive correlation determined between any of these elements. We observed Ti concentrations to average much lower than any measured element at 0.007 ± 0.001 mmol Ti kg^{-1} with the only occurrences of nanoparticulate Ti resulting from the Anoxic incubation and constituting 0, 3, 8, and 21% of <415 nm Ti for Fields 1, 2, 3, and 6 respectively. One of the three replications from the Anoxic incubation of Field 2 showed a Ti concentration that was much greater (0.105 mmol Ti kg^{-1}) than all of the other measurements and was therefore excluded in the calculation of the average Ti concentration and percent <415 nm Ti. We found Ca to be the most abundant element measured with an average of 8.75 ± 3.37 mmol kg^{-1} but only 5.6 % occurring as nanoparticulate Ca. No correlations were observed between any of these elements and P.

Transmission electron microscopy analyses indicate the presence of a broad particle size distribution in the 1 nm – 415 nm size fraction of soil incubations from Field 2 (Figure 3.6A). A qualitative inspection of micrographs taken at medium magnification (~50,000 X) shows particles that range from 20-100 nm. Closer inspection (Figure 3.6B) reveals particle regions with high and low electron densities. High resolution TEM on high- and low- electron dense regions (Figure 3.6C & D respectively) show the lighter, electron-poor region (Figure 3.5D) is dominated by Al and Si (consistent with an aluminosilicate) while the darker, electron-dense region is dominated by Fe and Ti. Transmission electron microscopy data is the elevated counts of P associated with the Fe and Ti rich particle regions. High resolution TEM micrographs from Field 6 also reveal many regions on particles that bear lattice fringes (Figure 3.7) which indicates crystallinity. These regions are dominated by Al and Si and, as expected, show little P.

Discussion

In our current work, we employ TEM to corroborate the size and composition of nanoparticles isolated by differential centrifugation. Transmission electron microscopy of soil incubation samples suggests many of the larger particles are actually aggregates of <10 nm Fe- and Ti-rich particles, 50 nm flakes of an aluminosilicate mineral—which we tentatively assigned to kaolinite—and in some images films of low-electron density material likely representative of organic matter. Phosphorus appears localized on the metal-oxide portions of these aggregates. Similar observations have been made in other soils (Arai and Sparks, 2001; Olli et al., 2009; Young and Ross, 2001).

The origin of nPP is an important consideration in this study. Released P concentrations were consistently below detection in the control plots (no poultry litter added). Thus, we assume the bulk of P in the soils comes from the litter amendments. The release of soil colloids and nanoparticles may result from changes in pH, Eh, soil solution chemistry, and decreases in ionic strength (Chorover and Sposito, 1995; Pokrovsky and Schott, 2002; Itami and Fujitani, 2005; Ryan and Gschwend, 1994; Thompson et al., 2006). Accompanying these changes are processes that may in turn cause *de novo* generation of nanoparticles, such as the precipitation of Fe^{III}-

oxides along redox boundaries (Ryan and Gschwend, 1990) which can be stabilized by dissolved organic matter (Liang et al., 1993). Our soil incubations demonstrate that the saturation of soils that contain high P loads will, as expected, release nPP into solution. We also see a significant increase of released nPP from soils after an extended period of anoxia, most noticeably in soils that are seasonally saturated. This significant increase is not observed by raising the pH above that observed at the conclusion of the anoxic period. This non response to increased pH corresponds with the findings of Rick and Arai (2011) in similar soils.

Our findings suggest that the reduction of an Fe oxide cement under anoxic conditions is what drives the release of nanoparticles for our study site. Ryan and Gschwend (1990 and 1992) drew the same conclusion from oxic and anoxic groundwater samples in Atlantic Coastal Plain soils of New Jersey and Delaware and from sediment cores from uplands and swamps of the New Jersey Coastal Plain respectively. However, Ryan and Gschwend (1994) later showed from samples of an Atlantic Coastal Plain aquifer of New Jersey that Fe oxide reductive dissolution was not needed to release nanoparitcles but rather that increasing electrostatic repulsion between nanoparticle surfaces can mobilize nanoparticles. Likewise, Thompson et al. (2006) showed from samples of a basaltic upland forest soil of Maui, Hawaii that the dynamics of nanoparticles were dependent on pH changes that accompanied redox oscillations instead of the changing solubility of Fe oxides.

More recent studies have focused on the mobilization of organic nanoparticles and bound entities due to increased pH. In wetland soils of Brittany, Western France, Pedrot et al. (2009) and Grybos et al. (2007) showed that many trace elements become mobilized due to increases in pH as these trace elements tend to be bound to organic nanoparticles. Subsequently, in the same area, Grybos et al. (2009) showed with these soils that organic matter solubilization was driven by increased pH rather than reducing conditions. Conversely, De-Campos et al. (2007) observed the stability of nanoparticles decreases and soluble Fe^{2+} increases as a function of increasing reduction time (from 1 h to 14 d) and decreasing Eh in seasonally ponded upland soils of Indiana that were both cultivated and uncultivated. However, pH and dissolved organic C generally increased as a function of reduction time in uncultivated fields. In cultivated fields, a similar relationship between reduction time and pH was observed but dissolved organic C concentrations were comparably low and appeared to be independent of reduction time.

In an 11 y old constructed wetland in the San Joaquin Valley of California, Maynard et al. (2009) showed that increased exposure to reducing conditions caused the dissolution of crystalline Fe oxides and formation of poorly crystalline Fe oxides at the sediment-water column interface which increased the P sorption capacity of the soil. In our study, however, TEM micrographs showed nanoparticles from soil incubation samples (Figures 3.6C & 3.7 respectively) that were strongly crystalline. Additionally, our TEM-electron dispersive spectroscopy are consistent with nanoparticles composed of aggregates of kaolinite and Fe and Ti-oxides with suggestions of an organic matrix, all of which are common constituents in these soils (Franklin et al., 2007; Pierson et al., 2001).

Conclusion

Our work agrees with the findings of Rick and Arai (2011) in similar soils in that nPP contributed little to P released under oxic conditions and that an increase in pH did not noticeably increase nPP. However, our work has demonstrated that brief periods of saturation can release noticeable amounts of nPP and extended periods of anoxia can release significant amounts of nPP. These released particles range from several nm's to greater than 400 nm's with an estimated mean diameter of 250 nm. Furthermore, we have observed this nPP released by soil incubations is primarily associated with 1 – 3 nm Fe- and Ti-oxide phases that aggregate with larger (~50nm) flakes of aluminosilicates and organic matter to form the composite particles.

These results join a large host of other relevant findings that serve to further increase our understanding of colloid and nanoparticle release in the environment, the size and composition of these particles in a given system, and their potential to bind and carry nutrients, metals and contaminants in and through a given system. The codification of a standard test and analytical procedure could contribute greatly to advancing our knowledge on the subject as Rick and Arai (2011) suggested, especially given that we are currently subjected to comparing the results of various test parameters and analytical methods. However, agreeing on a uniform procedure presents challenges in and of itself and such a procedure will take time to soundly develop and will, undoubtedly, change and improve over time. For now we relied on TEM which confirms that the size distribution of particles fit our stated range from our selected separation method. We also employed several methods of characterization commonly used and found broad-scale agreement, most noticeable between MRP via colorimetry and total P via ICP-MS.

Given that we do see nPP released into the soil solution in samples taken from this site, the next step is to determine to what extent this nPP is removed from the site via runoff and leachate resulting from natural occurrences. Also, thorough characterization of these particles, if found, should be conducted to increase our understanding of these particles and for comparison against those found in our present study. The pursuit of the aforementioned may serve to put our current findings in context with the system as a whole.

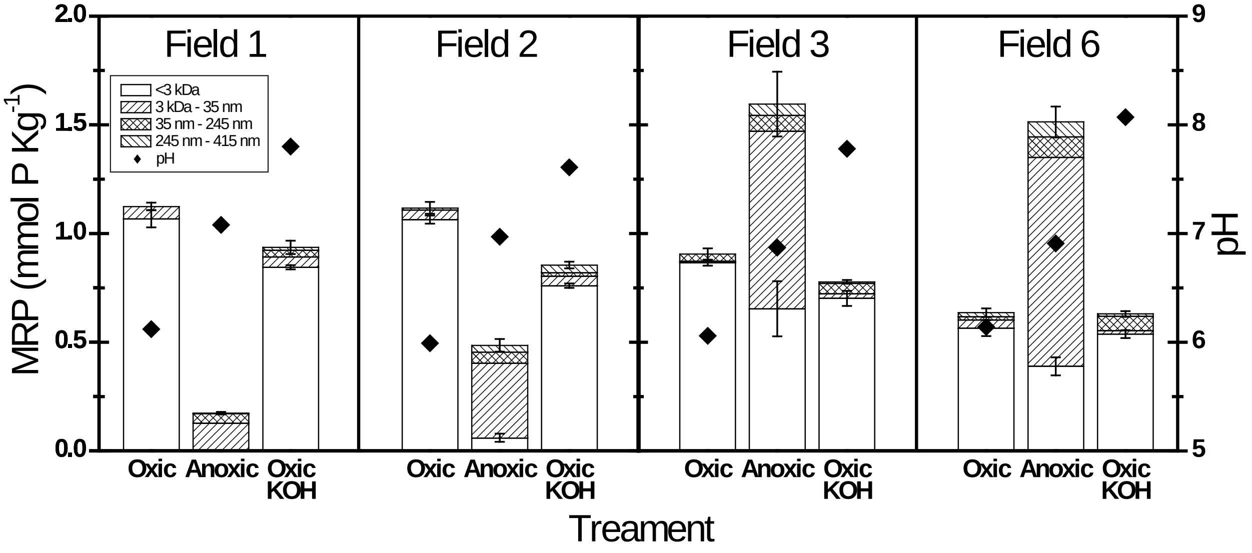

Figure 3.2. Molybdate reactive phosphorus (MRP) concentrations in solution from incubations of soil samples from Fields 1, 2, 3, & 6. Dissolved and nanoparticle size fractions are presented as stacked bars (left y-axis) and pH measurements are presented as dots (right y axis). Error bars shown for <450 nm and <3kDa fractions.

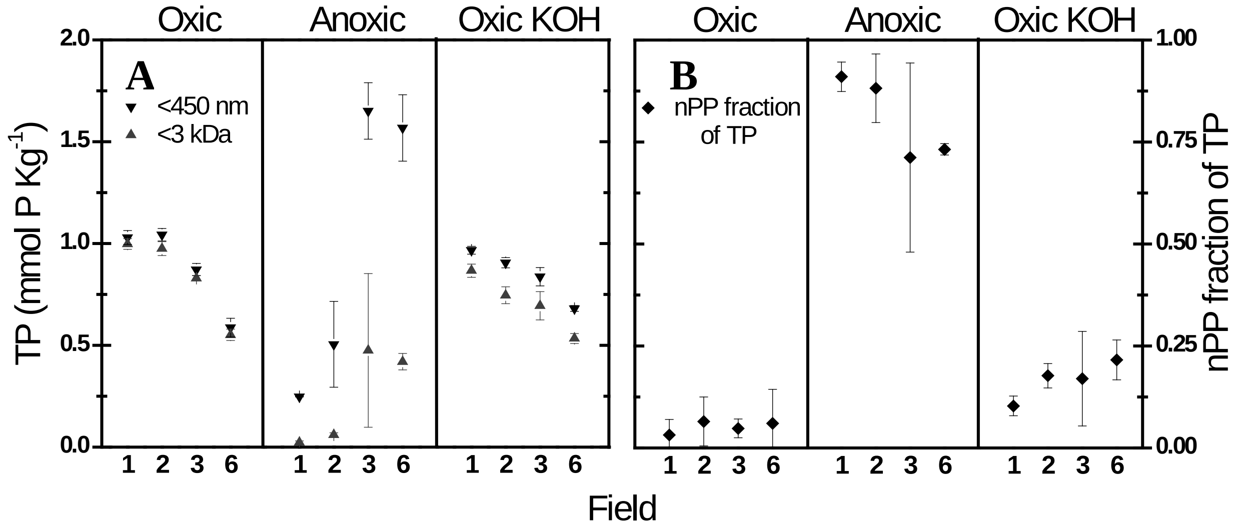

Figure 3.3. Total phosphorus (TP) concentrations in solution from incubations of soil samples from Fields 1, 2, 3, & 6. A) <415 nm and <3 kDa concentrations of TP. B) 3 kDa – 415 nm phosphorus (nPP) fraction in <415 nm TP.

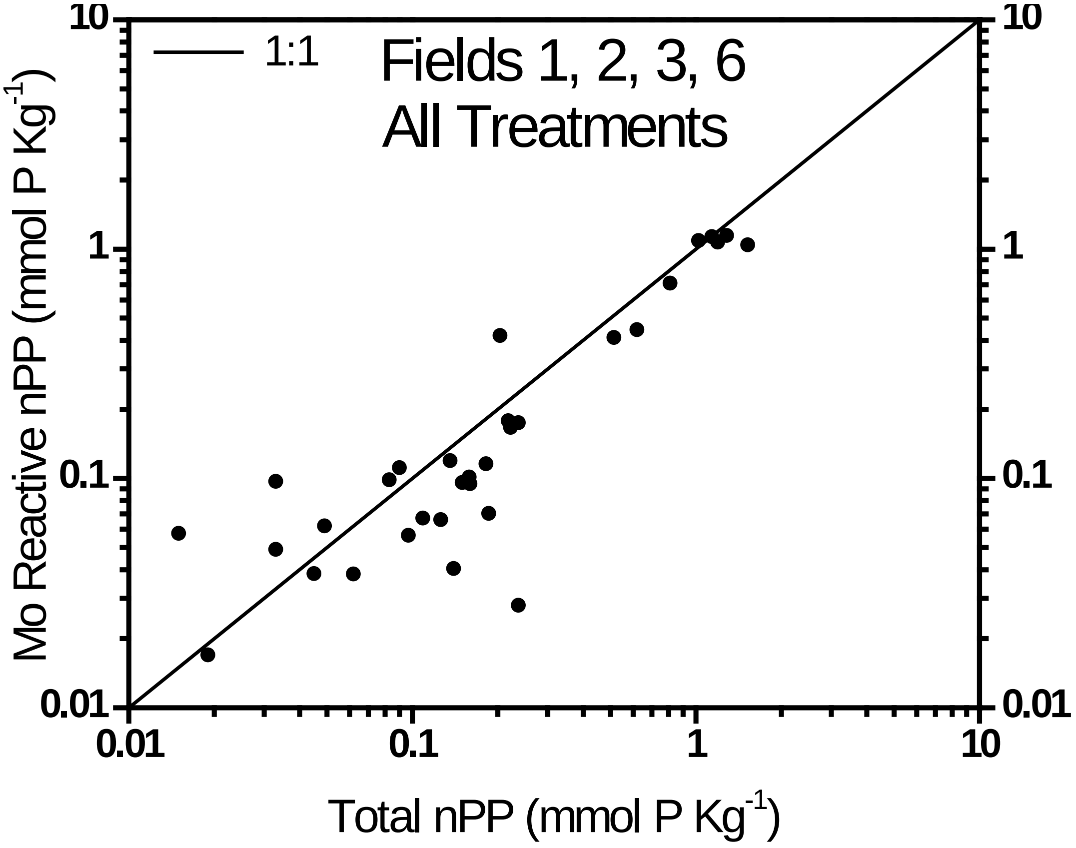

Figure 3.4. Comparison of total phosphorus (TP) and molybdate reactive phosphorus (MRP) measurements for nano-particle bound phosphorus (nPP) in solution of all incubations from fields 1, 2, 3, and 6. All replicates shown. Average error between methods 0.08 ± 0.09.

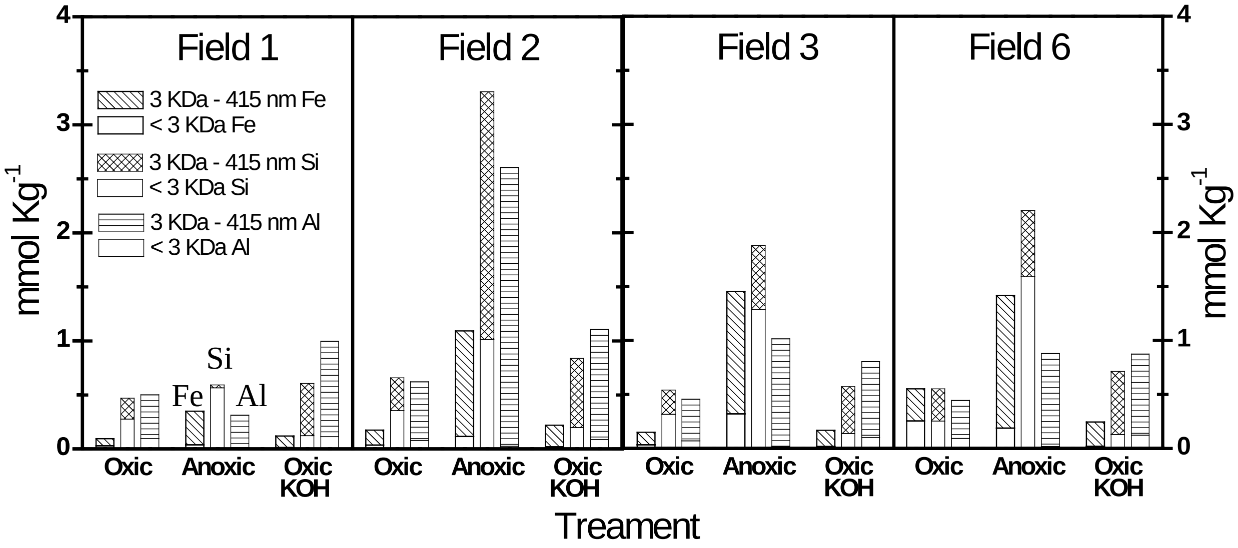

Figure 3.5. Concentration of total Fe, Si, & Al from incubations of soil samples from Fields 1, 2, 3, & 6. Dissolved and nanoparticle size fractions are presented as stacked bars.

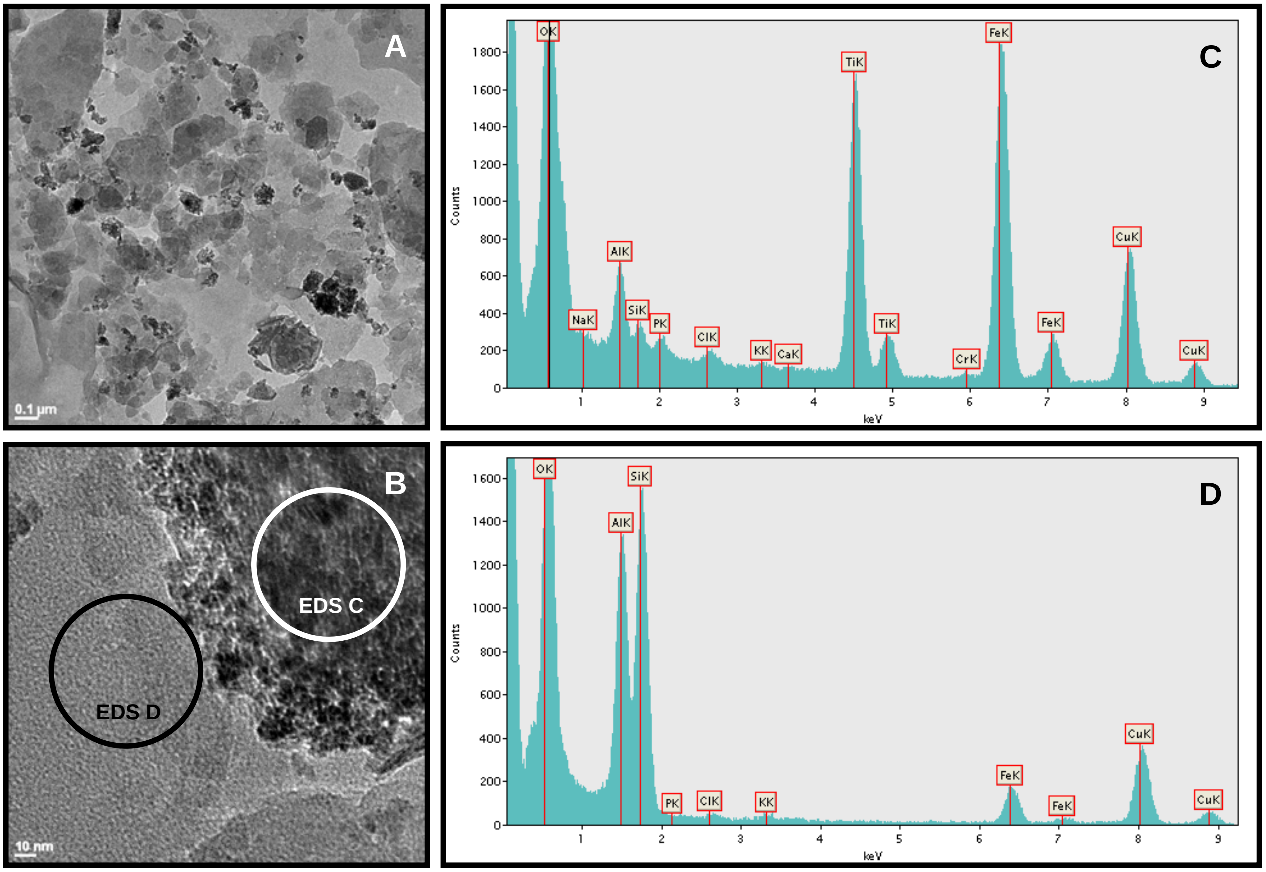

Figure 3.6. Transmission electron micrographs and energy dispersive X-ray spectroscopy analysis of Field 2 soil Anoxic incubations spun to remove < 415 nm particles and dialyzed to remove excess salts: A) micrograph shows the presence of minerals similar to those detected in runoff. B) a close-up of a mineral presenting distinctly different high and low density/contrast regions. A higher magnification EDS analysis of each region separately C) and D) present different elemental profile and suggests that P is associated with the high density region characterized by the presence of Fe.

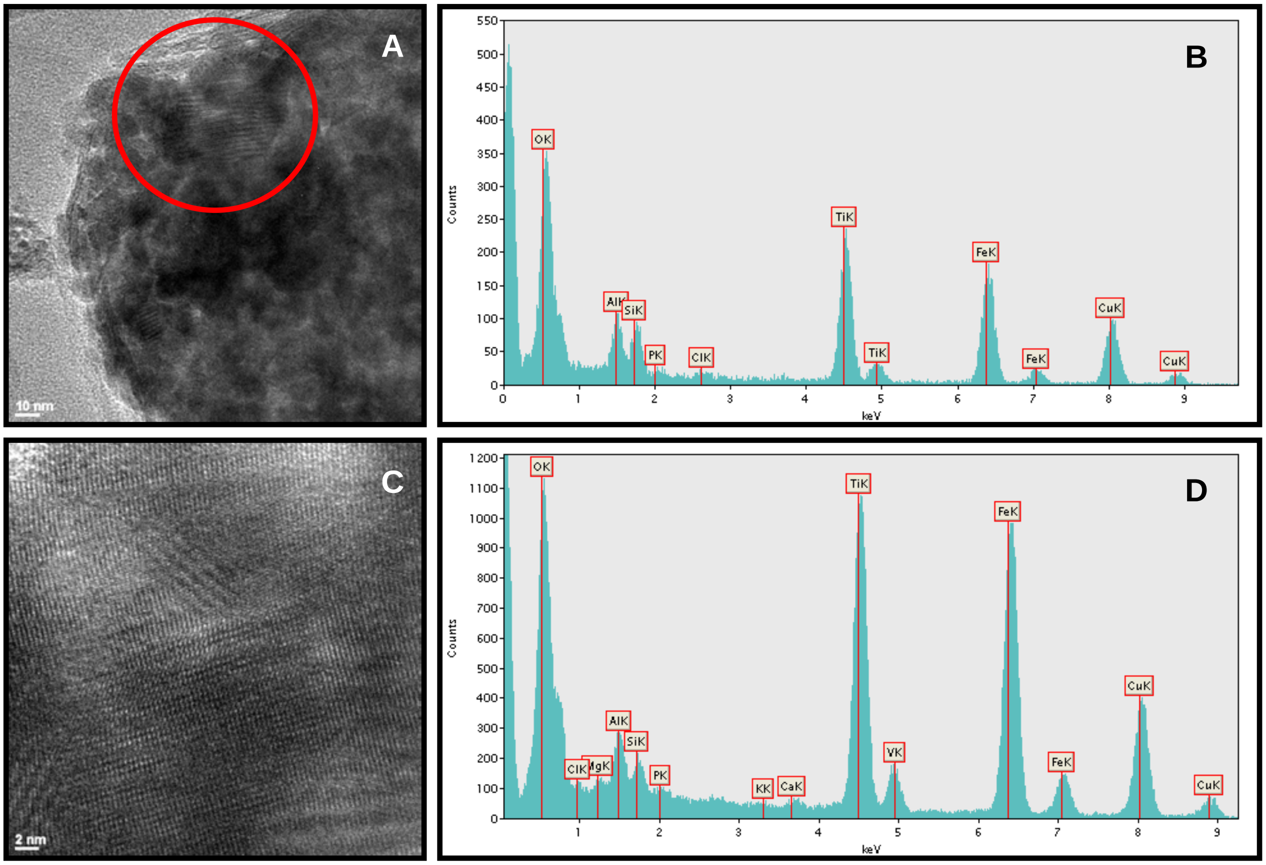

Figure 3.7. Transmission electron micrographs and energy dispersive X-ray spectroscopy of Field 6 soil Anoxic incubation spun to remove < 415 nm particles and dialyzed to remove excess salts: A) micrograph shows the presence of Al, Si, Ti, and Fe. Red circle in A) is magnified as micrograph C) and shows fringes indicating crystallinity.

CHAPTER 4

NANOPARTICLE-BOUND PHOSPHORUS IN RUNOFF OF POULTY-LITTER AMENDED GRASSLAND[1]

---

[1] Henderson, Russell D., N. Mantripragada, N. Kabengi, M. Cabrera, S. Hassan, A. Thompson,

To be Submitted to the Soil Science Society of America Journal

Abstract

Limiting P loss from poultry litter amended pastures preserves the vitality of nearby sensitive ecosystems. Standard sampling methodology separates particulate-bound P from “dissolved” P by a 0.45-μm filter. However, numerous particles that strongly sorb P are smaller than 0.45 μm, and if present, would be incorrectly counted with “dissolved” P. Given that these particles show vast differences in reactive-transport behavior than truly dissolved aquo-ions, misclassification may cause great errors in predictive models. Laboratory suspensions of P-rich soils from the Southeastern U.S. Piedmont have produced little to no particle-bound P under oxic conditions. However, some of the same suspensions did generate particle-bound P when subjected to prolonged anoxic conditions. The potential for this bound P to be removed from a system needs to be tested at the field scale. We measured concentrations of nanoparticle-bound P (nPP; 1 nm – 415 nm) in runoff P for a four-month period following a litter application (Nov. 2009) in six 0.8-ha fescue watersheds that had received bi-annual poultry litter applications since 1995. Samples were size fractionated by differential centrifugation, ultrafiltration, and field flow fractionation (FFF) and analyzed for Molybdate-reactive P (MRP), total P, Al, Fe, Si, Ti, and Ca. Selected samples were visualized via transmission electron microscopy (TEM) and energy dispersive X-ray spectroscopy (EDS). In the runoff, we found an average of only 10% (maximum of 21 ± 2.5%) of the <0.415 μm runoff P associated with nanoparticles. These nano-particles had a mean diameter of 250 nm and were composed of aggregates of ~50 nm aluminosilicate flakes with clusters of <10 nm Fe and Ti-rich phases which contained most of the P detected by EDS. In most cases, this nPP was effectively measured by the molybdate reaction method and thus it is likely previous studies characterizing “dissolved” P as MRP passing through a 0.45-μm filter have included nPP. Despite our findings that nanoparticles contributed little to P losses from

runoff in this system, it is critical to remember that the cultural practices of this system greatly hedge against erosion where many systems do not. Thus, a study of more highly erodible fields may show a greater significance in the contribution of nanoparticles to bind and transport P.

Introduction

Many studies have evaluated the effects of agricultural management practices on runoff volume, quality, and P losses (Butler et al., 2008; Franklin et al., 2006; Franklin et al., 2007; Kuykendall et al., 1999). The potential for P loss is accentuated when broiler litter is surface applied as a fertilizer and thus extensive research efforts have been directed toward evaluating the mechanisms of P loss and developing strategies for minimizing runoff P loss following broiler litter amendments (Butler et al., 2008; Franklin et al., 2006; Franklin et al., 2007). Preventing P transport to surface waters remains a central concern in mitigating the harmful effects of eutrophication on exposed water bodies. Standard methods for assessing P loss in runoff include separating mobilized P into “particulate-P” and “dissolved-P” via filtration through 0.45 μm (Haygarth and Sharpley, 2000). However, it is widely recognized that particles < 0.45 μm present some of the most abundant and reactive surfaces in soil and environmental systems (Hochella et al., 2008; Kretzschmar et al., 1999) on account of their high surface areas (>10 m^2 g^{-1}) and the high binding efficiency of metal-oxide or organic surface functional groups which are typically present. They can be potent carriers of metals, carbon, and nutrients—facilitating longer transport distances than would be predicted for dissolved ions (de Jonge et al., 2004; Heathwaite et al., 2005; Makris et al., 2006). Indeed, P strongly binds to high-surface area Fe and Al-bearing nanoparticles and organic matter, all of which have been implicated in P transport in river systems (Lin et al., 2009; Mayer and Jarrell, 1995; Olli et al., 2009). In soil surface runoff, Haygarth et al. (1997) have shown that as much as 15% of reactive P found in <0.45 µm filtrates does not pass through a 1000 Da (≈ 1 nanometer) ultrafilter and thus cannot be truly dissolved, ortho-phosphate. Also, Turner et al. (2004) have shown as much as 56% of P in surface runoff fell within the 1 nm – 1 µm range. Similarly, in fresh water surfaces, Filella et al. (2006) have shown up to 26% ± 6% of P fell within the 3000 Da – 1.2 µm range. In leachate from undisturbed soil columns of an agricultural field, de Jonge et al. (2004) showed that nanoparticles <0.24 µm were responsible for transporting around 75% of the P leached. Also, Haygarth et al. (1997) showed that the <1000 Da fraction did not accounted for 13% of total reactive P in soil leachate from grasslands. Additionally, Hens and Merckx (2002) have shown particles ranging from 0.025 µm – 0.45 µm comprised 40 – 58% of < 0.45 µm MRP in soil-water extracts from a sandy grassland and sandy arable field. However, Rick and Arai (2011) showed that particles 10-200 nm did not significantly contribute to P transport in Ultisols from South Carolina agricultural fields containing high P loads before and after these soils underwent significant pH increases. Still, particle transport of P from such sites should be measured to see if this is expressed at the field scale under field conditions

We selected a site that has received broiler litter amendments bi-annually for 12 of the last 15 years and contains fields that are and are not seasonally saturated to study P release and transport. Thus, our study objectives are (i) to determine the extent of nanoparticle-bound P (nPP) contribution to released Molybdate-reactive P (MRP) in pasture runoff from well drained and poorly drained sites and (ii) to characterize the size and composition of these nanoparticles. We hypothesized nPP to be a significant portion of MRP loss in runoff.

Materials and Methods

For our assessment of nPP, we selected a well-instrumented poultry litter amended grassland at the Central Georgia Research and Education Center in Eatonton, GA that has shown considerable losses of dissolved reactive P during previous runoff events (Franklin et al., 2006; Franklin et al., 2007; Kuykendall et al., 1999; Pierson et al., 2001). Nanoparticles from collected runoff were size fractionated using a combination of differential centrifugation and ultrafiltration. Nanoparticle characterization was carried out by inductively coupled plasma-mass spectrometry (ICP-MS), transmission electron microscopy (TEM), and field flow fractionation (FFF) coupled with multi-angle-light-scattering (MALS) and in-line detection via ICP-MS.

We collected runoff for a four-month period following a litter application (Nov. 2009) from ten 0.8-ha, fescue/bermudagrass hay fields described in Chapter 3, Materials and Methods. Each field is enclosed by an earthen berm that channels surface runoff to a 0.45-m flume where it is collected by an ISCO 3700FR refrigerated sampler (ISCO, Lincoln, NE) (Franklin et al., 2007).

Collected runoff water was separated as described in Chapter 3, Materials and Methods. Additionally, field flow fractionation (FFF) was employed on unacidified runoff samples for nanoparticle characterization (see section 2.5 below).

We determined molybdate-reactive phosphorus (MRP) on all subsamples via the molybdate blue method (Murphy and Riley, 1962) with ultraviolet detection on a Shimadzu UV-1700 UV-Visible Spectrophotometer using a method detection limit of 0.4 ppm. The <415 nm and <3kDa separates of runoff events 1-6 were also analyzed for total P, Al, Fe, Si, Ti and Ca on a Perkin Elmer-Sciex 9000 ICP-MS.

Transmission electron microscopy characterization was carried out on unacidified <415 nm subsamples from selected runoff samples. Runoff samples from Event 2 on Field 2 and 5 were selected because these events exhibited high levels of nPP. The runoff samples from Field 2 were imaged without removal of dissolved salts, while the runoff sample from Field 5 was dialyzed (1 kDA, Spectrapor) against 1.7 x 10^5 Ω-m water decreasing the electrical conductivity of the runoff water from 220 μS m^{-1} to 17.0 μS m^{-1}. Samples were prepared by depositing one to three drops of the samples on a copper specimen grid coated with an ultrathin layer of carbon (Ted Pella, Inc.) and allowing the water to evaporate in a laminar flow hood. Images were obtained using a JEOL 2010F Transmission Electron Microscope operating at 200 kV (JEOL Ltd, Tokyo Japan). Information on the sample elemental compositions was collected using energy dispersive X-ray spectroscopy (Oxford detector).

In addition, unacidified <415 nm separates from runoff Event 2 were analyzed for particle size and elemental composition via FFF coupled with MALS in-line detection via ICP-MS. In-line particle separation was achieved with a Wyatt Eclipse-2 FFF system running a 7.75” X 2.19” channel with 350M spacer and 10 kDa cellulose membrane. The mobile phase buffer (pH 7.5) was prepared from 1.8 x 10^5 Ω-m H_2O with 10^{-3} mol L^{-1} NH_4NO_3, 3 x 10^{-4} mol L^{-1} sodium dodecyl sulfate and 200 mg L^{-1} sodium azide. Channel flow was constant at 0.9 mL across the 39-min runtime with an initial 8 min of sample focusing of a 100 μl injection followed by 31 min of separation where the cross-flow rate gradient was varied in the following manner: step (1) gradient 0.5 to 0.3 mL min^{-1} for 7.5 min; step (2) gradient 0.2 to 0.1 mL min^{-1} for 12 min; step (3) gradient 0.1 to 0 mL min^{-1} for 6 min; step (4) no crossflow for 5.5 min. Effluent from the FFF was coupled to a Wyatt Dawn Heleos® MALS detector and Quasi-Elastic Light Scattering detection. Spectral analysis was done using Astra® software (Dubascoux et al., 2008).

Results

The majority of runoff P (~ 90%) passed through the 3kDa filters. Consistent with prior results from these fields (Franklin et al., 2007), <415 nm MRP (Figure 4.2) and total P (Figure 4.3) concentrations were highest during the first month of runoff (Events 1 and 2) following litter application and decreased during subsequent runoff events. However, the concentration of nPP was unrelated to the time after litter application, ranging from 0 to 2.67 mg L^{-1}, with an average concentration across all fields of 0.90 ± 0.65 mg L^{-1}. Nanoparticle-bound P was most abundant, although highly variable, in the 3kDa – 35 nm particle size fraction. In fact, average molybdate (Mo) reactive nPP decreased slightly as a function of increasing particle size with averages across all samples of 0.4 ± 0.4 mg L^{-1}, 0.2 ± 0.4 mg L^{-1}, and 0.2 ± 0.5 mg L^{-1} for the 3kDa – 35 nm, 35nm – 260 nm, and 260 nm – 415 nm particle size fractions, respectively. At the same time, the largest nPP concentrations were observed in the 260 – 415 nm fraction (2.6 ± 0.3 mg L^{-1}) compared with 1.5 ± 0.2 mg L^{-1} for 3kDa – 35 nm. Several runoff events contained no measurable Mo reactive nPP. Furthermore, analysis of total P in runoff Events 1-6reveals much of the nPP is molybdate reactive (Figure 4.4). Cumulative runoff from fields 1-6 for all nine observed runoff events was 122, 242, 189, 200, 209, and 293 mm respectively (Table 3.1).

We assessed the molar abundance of nanoparticle Fe, Si, Al, Ti, & Ca in runoff Events 1-6. Here, nanoparticle Fe, Al, and total P concentrations were within an order of magnitude of each other while nanoparticle Ti concentrations were much lower and well correlated in both the dissolved and nanoparticulate fractions. In some cases the nanoparticle total P was close to or even greater than the nanoparticle Fe or Al. This could suggest either discrete Al-P or Fe-P minerals or a large molar abundance of organic matter in the nanoparticles. Generally, Si and Ca were dissolved and observed values were similar to corresponding total P values.

Transmission electron microscopy analyses indicate the presence of a broad particle size distribution in the < 415 nm size fraction of Field 2 (Figure 4.5A). A qualitative inspection of micrographs obtained at medium magnification (~50,000 X) reveals particles ranging from 20-100 nm. Electron dispersive spectroscopy analysis (Figure 4.5B) of the region captured on the presented micrograph show that in addition to the background salt present (Ca, Na, Cl, K, Mg, S) this sample contains Al, Si, Fe, Ti, and P. The micrographs reveal particle regions with high and low electron densities (darker or lighter image contrast). Higher electron-dense regions correspond with heavier elements, whereas the low electron-dense regions are consistent with organic matter. Using High Resolution TEM, we investigated a high electron density region (Figure 4.5C) that presented an aggregation of 2-10 nm Fe- and Ti-rich individual nanoparticles (Figure 4.5D). Additionally, the High Resolution TEM micrographs reveal many regions bearing lattice fringes, indicating the presence of crystalline phases with parallel crystallographic axes in this area.

Decreasing the dissolved ion concentration by dialysis improved the clarity of the particle images (Figure 4.6A and 4.6B) and removed the background electrolyte peaks in the electron dispersive spectroscopy spectra (Figure 4.6C and 4.6D). Moreover, dialysis allowed us to isolate the region of the nanoparticle aggregates harboring elevated levels of P. Many regions of the micrographs contain clearly separate electron-dense and electron-poor regions (e.g., Figure 4.6B). Using High Resolution TEM, we collected distinct electron dispersive spectra from high- and low- electron density regions (Figure 4.6C and 4.6D, respectively). The lighter, electron-poor region (Figure 4.6D) is dominated by Al and Si. This is consistent with an aluminosilicate such as kaolinite, which are common in these soils. The electron-dense region (Figure 4.6C) is dominated by Fe and Ti, with much lower levels of Al and Si that may result from bleed-through of the underlying aluminosilicate. Interestingly, the P counts are nearly an order of magnitude higher in the electron-dense region. This association of high P counts with Fe and Ti rich particle regions was common across these micrographs.

FFF-MALS data are consistent with the differential centrifugations in that nanoparticle concentrations are highly variable between fields and runoff events, although the size distribution of the nanoparticles appears similar across most samples. FFF-MALS indicates a broad range of particle sizes forming a continuum of hydrodynamic radii from 30 nm to 280 nm with a peak radius at ~175 nm (Figure 4.7). FFF-ICP-MS data was typically consistent across this range of particle size and indicates these particles are primarily composed of Al and Si with secondary contributions of Fe and Ti and small quantities of P (Figure 4.7).

Discussion

We utilized FFF-MALS and TEM to confirm the size and composition of nanoparticles isolated by differential centrifugation. There is broad-scale agreement between these techniques. Transmission electron microscopy of runoff samples suggests many of the larger particles are actually aggregates of <10 nm Fe- and Ti-rich particles, 50 nm flakes of an aluminosilicate mineral—which we tentatively assigned to kaolinite—and in some images films of low-electron density material likely representative of organic matter. Consistent with our TEM work, FFF-MALS data suggest a broad particle size distribution with a mean particle size of ~300nm and particles rich in Al and Si with secondary concentrations of Fe and Ti, and minor P contributions on some samples. Phosphorus seems contained on the metal-oxide sections of these aggregates. Similar observations have been made on water and sediment samples from river systems (Lin et al., 2009; Pokrovsky and Schott, 2002).

The source of the runoff nanoparticles is an essential concern to this study. Runoff P concentrations were consistently below detection in the control plots (no poultry litter added). Therefore, we assume the majority of P in the runoff results from the litter amendments. Interestingly, while the first runoff event contained high levels of <415 nm P, we detected comparably little nPP (Fig. 1); conversely, later runoff events generally had lower <415 nm P concentrations and a greater abundance of nPP. Thus, the time after litter application appears unrelated to Mo reactive nPP concentration. Our data also showed no correlation between Mo reactive nPP and runoff volume per event ($R^2 = 0.26$, $P = 0.058$, $N = 54$). Rainfall intensity was not measured in this study, but previous work has generally found the greatest soil and P losses coincide with larger rainfall events (Edwards and Owens, 1991; Haygarth et al., 2006). However, other factors can yield wide variations in the amount of soil and P loss from equally intense rainfall events (Miller et al., 2009). The release of soil nanoparticles can occur due to changes in pH, Eh, decreases in ionic strength or changes to the solution composition (Chorover and Sposito, 1995; Pokrovsky and Schott, 2002; Itami and Fujitani, 2005; Ryan and Gschwend, 1994; Thompson et al., 2006). Included in this are processes that might cause *de novo* generation of nanoparticles, such as the precipitation of Fe^{III}-oxides along redox boundaries (Ryan and Gschwend, 1990) which can be stabilized by dissolved organic matter (Liang et al., 1993).

Agricultural management practices clearly affect surface runoff and erosion potential but are strongly influenced by field-specific factors. For instance, at our same study site, Franklin et al. (2007) found slit-aerating perpendicular to field contours decreased surface runoff and P losses only on well-drained fields and even appeared to increase surface runoff and P losses on poorly-drained fields. We found no correlation between aeration practices or field drainage characteristics and nPP. This may be due to the inherent difficulty of achieving good statistical separation of nPP from dissolved P when nPP values are <21% and calculated via the difference of two proportionally large numbers (<3kDa MRP and <415nm MRP). Otherwise it may indicate that the mechanisms controlling the release of P-rich nanoparticles are not related to field aeration treatment or soil drainage class. In other pasture systems, nPP was observed to comprise greater than 50% of the <450 nm MRP (Haygarth et al., 1997). Testing the influence of field management practices (i.e., aeration vs. no aeration) would likely be more tractable in systems with a higher nPP load than our current plots.

Conclusion

Our work has shown up to 21% of <0.415 µm runoff MRP from poultry litter-amended pastures is actually present as P-bound to nanoparticles (nPP) that range from several nm's to greater than 400 nm's with an estimated mean diameter of 250 nm. We have shown this runoff nPP is mainly coupled with 1 – 3 nm Fe- and Ti-oxide phases that aggregate with larger (~50nm) flakes of aluminosilicates and organic matter to form the composite particles. A key question emerging from this work is how misclassification of nPP as "dissolved" P would lessen our correct understanding of P release. There is some evidence to suggest the release of nPP may be accelerated relative to desorbed P, while exhibiting reduced bioavailability (Ekholm, 1994; Sonzogni et al., 1982). More broadly, our work and that of others (e.g., Gimbert and Worsfold, 2009; Haygarth et al., 1997; Hens and Merckx, 2001; Hens and Merckx, 2002) suggests closer inspection of classically-defined (e.g., <0.45µm) "dissolved" P across a greater number of sites may be a necessary next-step toward effectively managing P in our agricultural systems.

Table 4.1 Measured runoff (mm) for study period. Litter applied 11/5/2009.

	Runoff Event									
	1	2	3	4	5	6	7	8	9	
Date	11/22	12/2	12/9	12/15	12/18	12/25	1/17	1/25	2/5	
Field										Cumulative
1	0.8	22.9	1.6	0.4	27.0	20.2	12.0	19.4	17.7	122.0
2	2.3	37.9	0.0	2.9	64.1	37.5	22.0	38.9	36.4	242.0
3	2.1	36.4	2.9	0.8	40.4	31.4	18.8	29.5	27.1	189.4
4	2.0	37.8	3.6	0.8	43.5	32.4	20.7	30.2	28.9	199.9
5	4.0	39.1	2.8	2.0	45.5	33.5	18.0	33.1	30.8	208.8
6	11.8	52.2	0.0	5.9	57.1	43.3	42.6	39.9	40.3	293.1
7	4.4	37.0	4.4	0.0	0.0	34.3	23.9	28.7	28.3	161.0
8	3.6	40.3	6.0	1.6	46.0	40.0	27.1	34.2	33.8	232.6
9	5.7	39.4	5.7	2.8	44.0	34.2	21.6	30.2	31.3	214.9
10	10.5	52.7	0.0	0.0	53.5	37.6	24.6	32.9	31.8	243.6

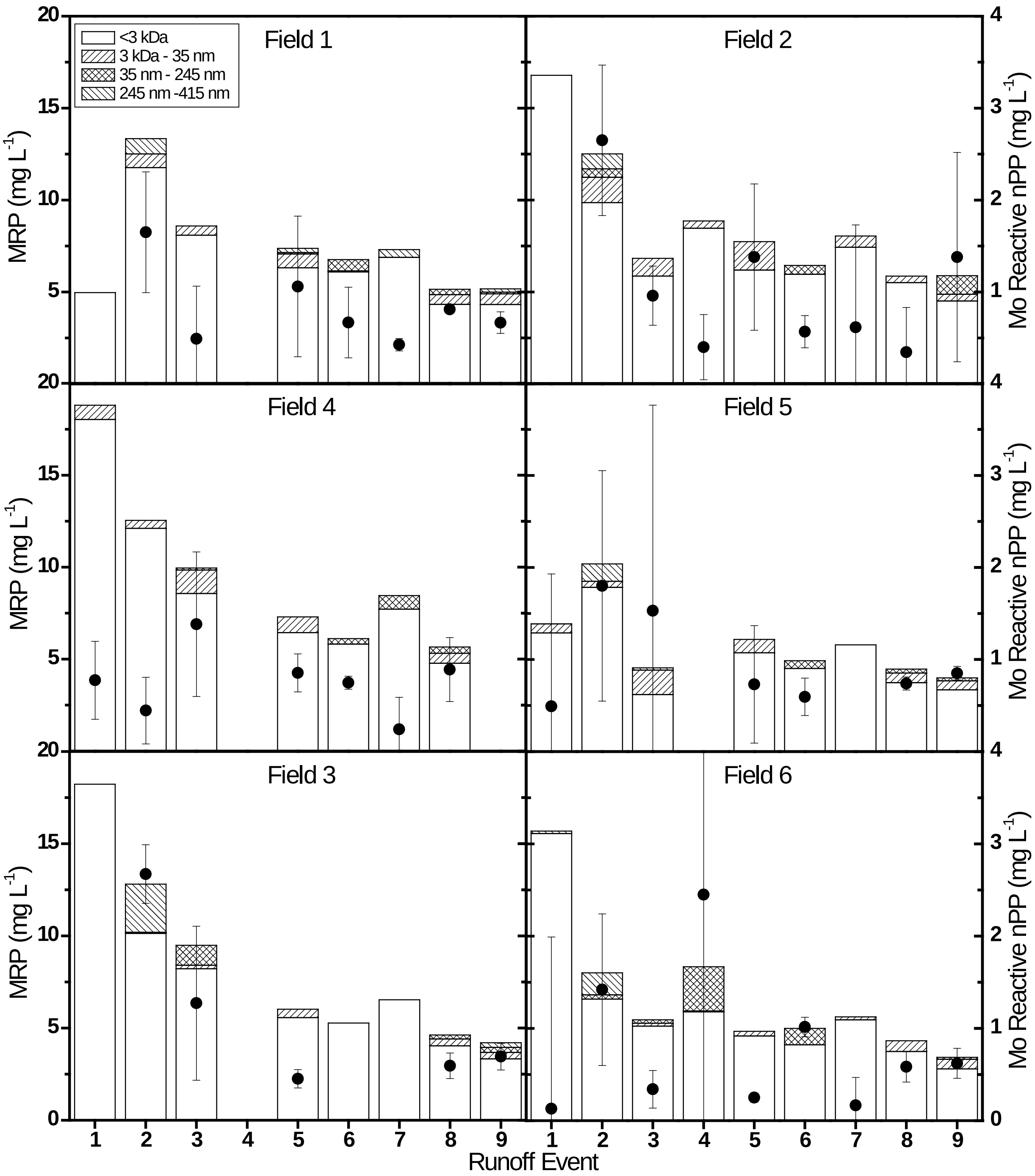

Figure 4.1. Molybdate reactive phosphorus (MRP) concentrations in runoff from litter amended fields for each runoff event during the study period. Dissolved and nanoparticle size fractions are presented as stacked bars (left y-axis) and Mo reactive nPP calculated as the difference between the <415 nm and <3kDa measurements are presented as dots (right y axis). Error bars are one standard deviation of duplicates.

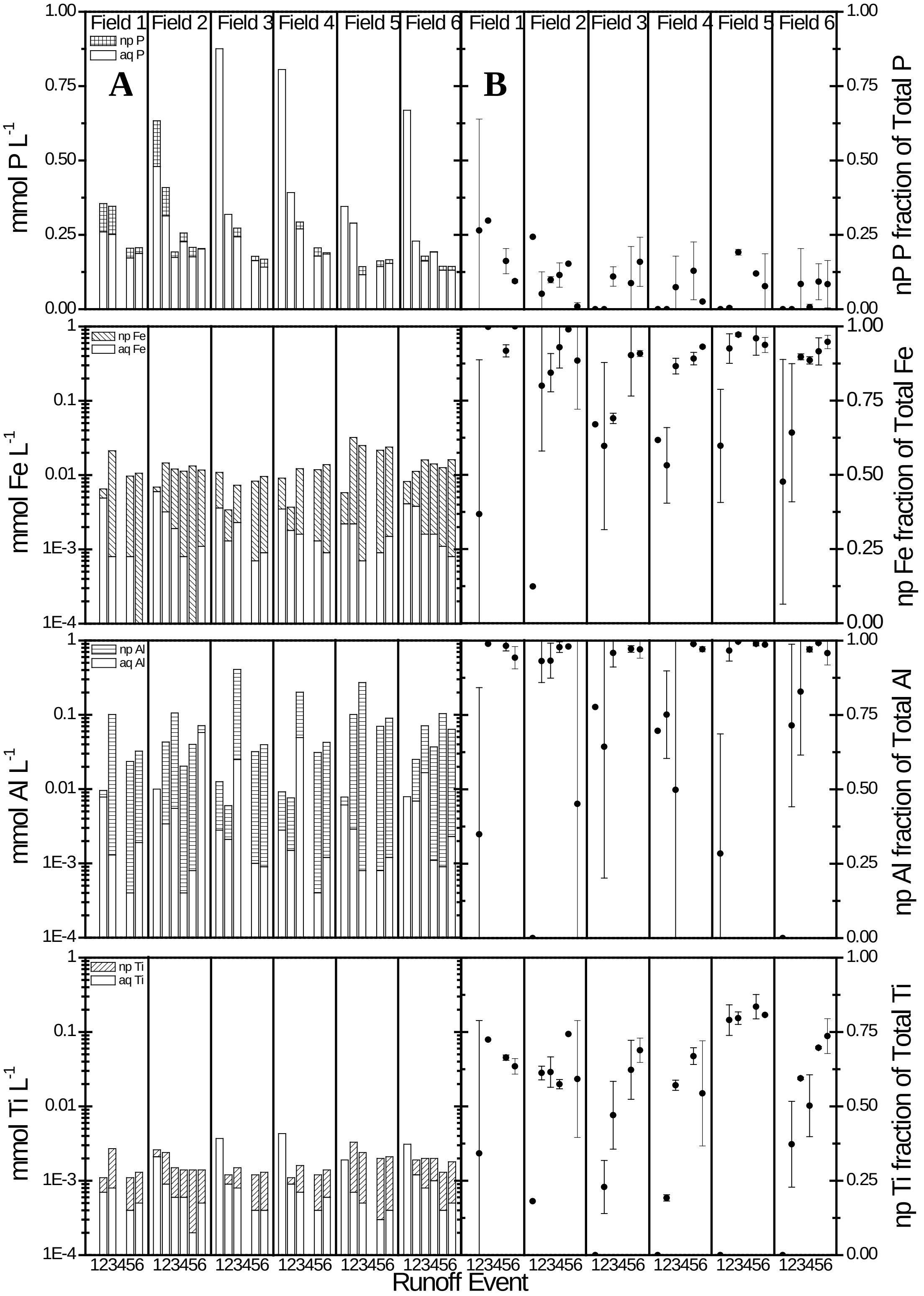

Figure 4.2. Concentration of total P, Fe, Al, Ti from runoff events 1-6 for Fields 1-6. A) <3 kDa (aq) and 3 kDa – 415 nm (np) concentrations presented as stacked bars . B) 3 kDa – 415 fraction in <415 nm sample.

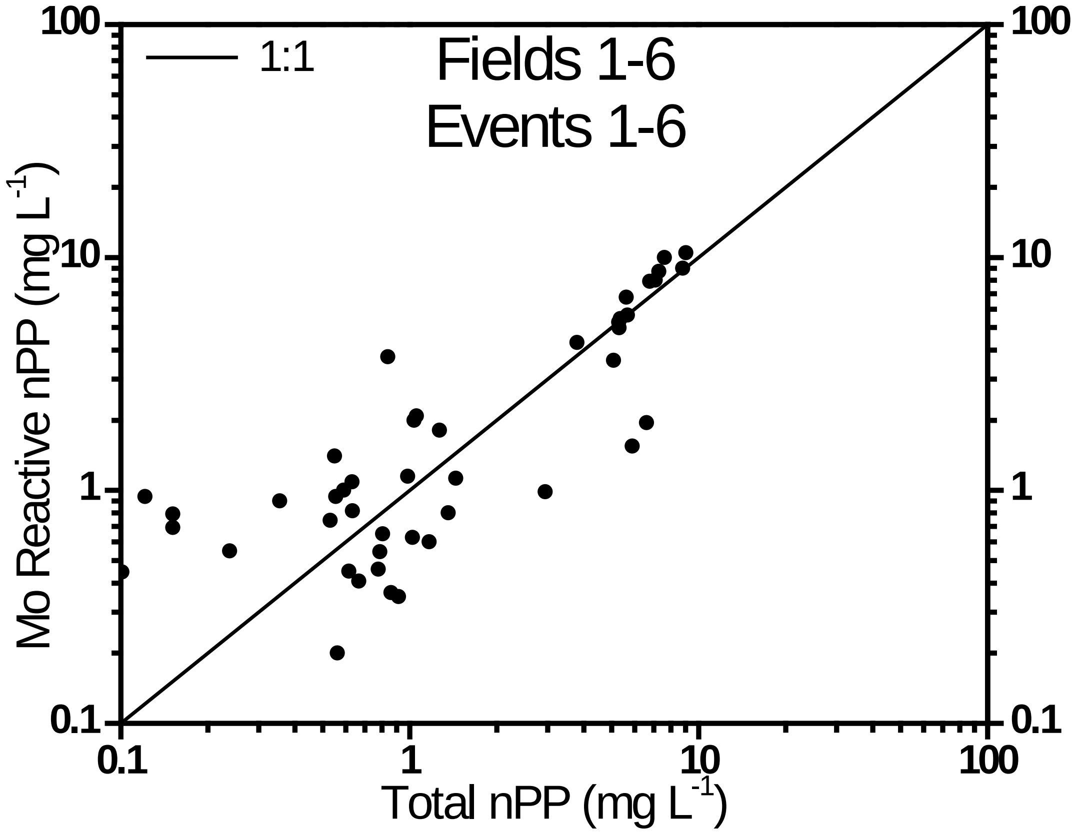

Figure 4.3. Comparison of total phosphorus (TP) and molybdate reactive phosphorus (MRP) measurements for nano-particle bound phosphorus (nPP) in runoff events 1-6 collected from fields 1-6. All replicates shown.

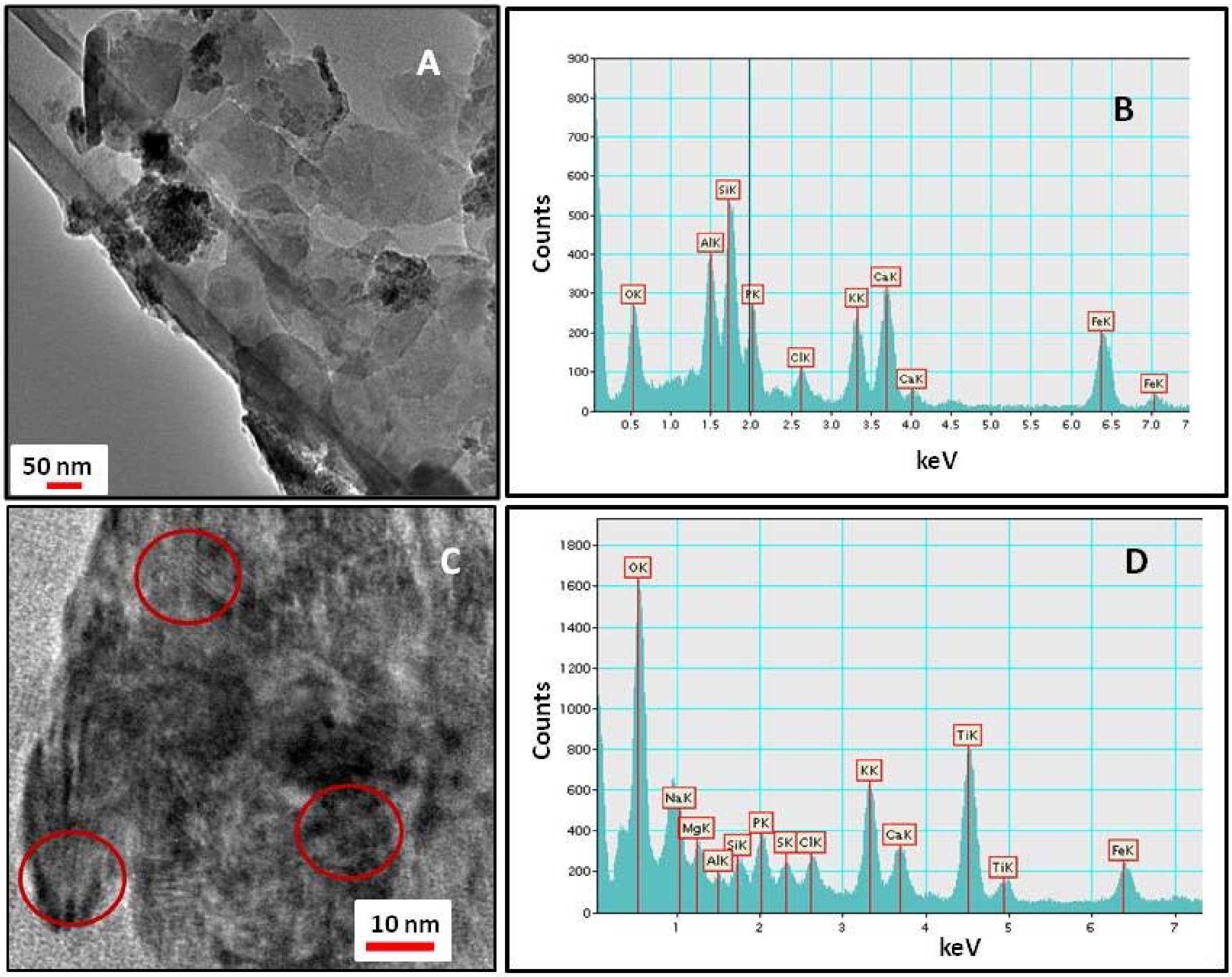

Figure 4.4. Transmission electron micrographs and corresponding energy dispersive X-ray spectroscopy analysis of: A & B) Field 2, runoff event 2 sample with only < 415 nm particles; C& D) Field 2, runoff event 2 sample spun to remove >415 nm and < 3000 Da particles. Both micrographs show the presence of minerals containing Al, Si, Fe and Ti, along with P and Na, Ca and K salts. Areas of micrograph C highlighted in red circles delineate crystal lattice fringes detected at the higher magnification. These represent the signature of crystalline minerals of nanoscale size present in the sample.

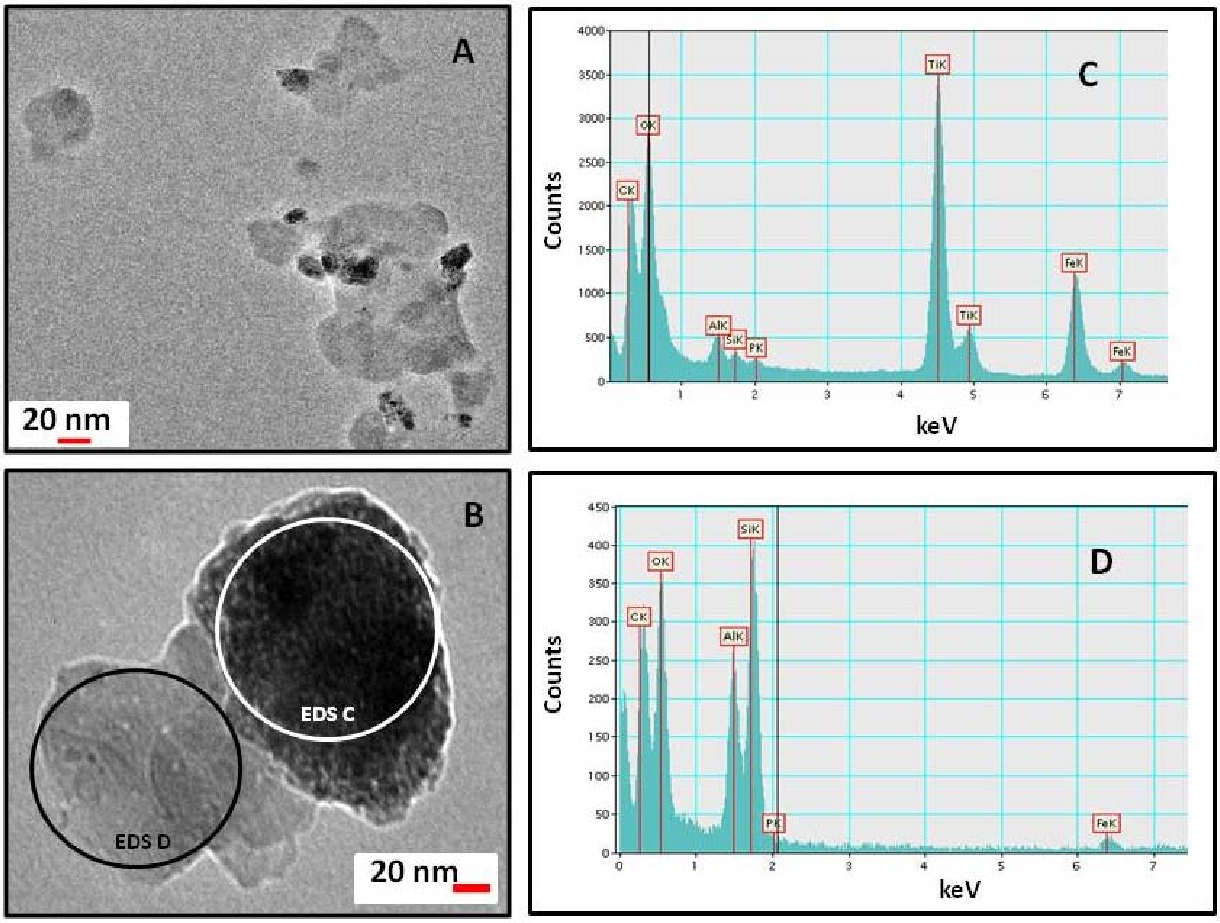

Figure 4.5. Transmission electron micrographs and energy dispersive X-ray spectroscopy analysis of Field 5, runoff event 2 sample spun to remove < 415 nm particles and dialyzed to remove excess salts: A) micrograph shows the presence of minerals similar to those previously detected; B) a close-up of a mineral presenting distinctly different high and low density/contrast regions. A higher magnification EDS analysis of each region separately C) and D) present different elemental profile and seems to suggest that P is associated with the high density region characterized by the presence of Fe, Ti, Al and Si.

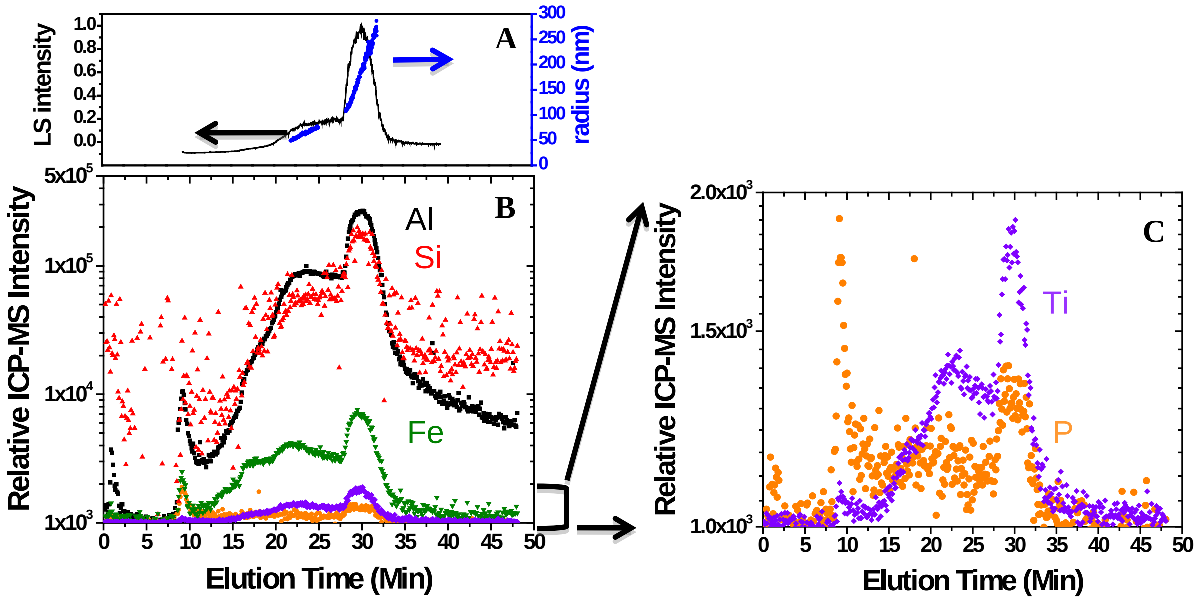

Figure 4.6. Asymmetric-flow field flow fractionation coupled to multi-angle light scattering detector and ICP-MS data from runoff samples. A) Hydrodynamic radius of nanoparticles. B) Al, Si, Fe intensity; C) Ti and P intensity.

CHAPTER 5

SUMMARY AND CONCLUSION

Increasing our understanding of nutrient activity and movement in and out of agricultural systems is vital as it will allow us to derive methods to increase the productivity of our agricultural lands while enabling us to better preserve the natural state of waters associated with the watersheds of these lands. Phosphorus is one such nutrient that has received considerable attention due to its potential to be a limiting factor in plant production, its abundance in readily available soil amendments such as poultry litter, and its potential to adversely affect sensitive bodies of water if improperly managed. In Georgia, this holds true due to the predominance of highly weathered soils, a thriving broiler industry, and a vast area of surface waters found in this state. Thus, we set out to better understand P losses associated with the common regional practice of frequently amending grasslands with poultry litter. Our work has shown that brief periods of saturation can release measureable quantities of nPP from the soils found in these grasslands, and that extended periods of anoxia can release significant quantities of nPP from these soils. We also found that up to 21% of <0.415 µm runoff MRP from these poultry litter-amended pastures is actually present as P-bound to nanoparticles (nPP) that range from several nm's to greater than 400 nm's with an estimated mean diameter of 250 nm. In addition, we have shown this runoff nPP and that released by soil incubations is primarily associated with 1 – 3 nm Fe- and Ti-oxide phases that aggregate with larger (~50nm) flakes of aluminosilicates and organic matter to form composite particles. This is significant given that the measureable losses of nPP shown in our work come from an agricultural system in which minimal erosion is expected. More work then should be conducted on sites that have animal litter surface applied and are more prone to erosion as these sites may show considerable nPP loss during runoff events. Also, anoxic laboratory incubations on soils in which pH is not allowed to change are needed to better isolate the contribution of anoxic conditions on a soil. Additionally, the relationship between the time a soil is anoxic and nPP release needs to be investigated. Future work should aim to increase our understanding of nutrient activity and movement through chemical and physical processes in agricultural systems to enable us to better manage these systems.

REFERENCES

Arai Y., Sparks D.L. (2001) ATR-FTIR spectroscopic investigation on phosphate adsorption mechanisms at the ferrihydrite-water interface. J. Colloid Interface Sci. 241:317-326.

Butler D.M., Franklin D.H., Cabrera M.L., Tasistro A.S., Xia K., West L.T. (2008) Evaluating aeration techniques for decreasing phosphorus export from grasslands receiving manure. J. Environ. Qual. 37:1279-1287.

Chorover J., Sposito G. (1995) Colloid chemistry of kaolinitic tropical soils. Soil Sci. Soc. Am. J. 59:1558-1564.

De-Campos A.B., Mamedov A.I., Huang C.H. (2009) Short-term reducing conditions decrease soil aggregation. Soil Sci. Soc. Am. J. 73:550-559.

de Jonge L.W., Moldrup P., Rubaek G.H., Schelde K., Djurhuus J. (2004) Particle leaching and particle-facilitated transport of phosphorus at field scale. Vadose Zone J. 3:462-470.

Dubascoux S., Von Der Kammer F., Le Hecho I., Gautier M.P., Lespes G. (2008) Optimisation of asymmetrical flow field flow fractionation for environmental nanoparticles separation. J. Chromatogr. A 1206:160-165.

Edwards W.M., Owens L.B. (1991) Large storm effects on total soil-erosion. J. Soil Water Conserv. 46:75-78.

Ekholm P. (1994) Bioavailability of phosphorus in agriculturally loaded rivers in southern finland. Hydrobiologia 287:179-194.

Filella M., Deville C., Chanudet V., Vignati D. (2006) Variability of the colloidal molybdate reactive phosphorous concentrations in freshwaters. Water Res. 40:3185-3192.

Franklin D.H., Cabrera M.L., Calvert V.H. (2006) Fertilizer source and soil aeration effects on runoff volume and quality. Soil Sci. Soc. Am. J. 70:84-89.

Franklin D.H., Cabrera M.L., West L.T., Calvert V.H., Rema J.A. (2007) Aerating grasslands: Effects on runoff and phosphorus losses from applied broiler litter. J. Environ. Qual. 36:208-215.

Gimbert L.J., Worsfold P.J. (2009) Temporal variability of colloidal material in agricultural storm runoff from managed grassland using flow field-flow fractionation. J. Chromatogr. A 1216:9120-9124.

Grybos M., Davranche M., Gruau G., Petitjean P. (2007) Is trace metal release in wetland soils controlled by organic matter mobility or Fe-oxyhydroxides reduction? J. Colloid Interface Sci. 314:490-501.

Grybos M., Davranche M., Gruau G., Petitjean P., Pedrot M. (2009) Increasing pH drives organic matter solubilization from wetland soils under reducing conditions. Geoderma 154:13-19.

Haygarth P.M., Sharpley A.N. (2000) Terminology for phosphorus transfer. J. Environ. Qual. 29:10-15.

Haygarth P.M., Warwick M.S., House W.A. (1997) Size distribution of colloidal molybdate reactive phosphorus in river waters and soil solution. Water Res. 31:439-448.

Haygarth P.M., Bilotta G.S., Bol R., Brazier R.E., Butler P.J., Freer J., Gimbert L.J., Granger S.J., Krueger T., Macleod C.J.A., Naden P., Old G., Quinton J.N., Smith B., Worsfold P. (2006) Processes affecting transfer of sediment and colloids, with associated phosphorus, from intensively farmed grasslands: an overview of key issues. Hydrol. Process. 20:4407-4413.

Heathwaite L., Haygarth P., Matthews R., Preedy N., Butler P. (2005) Evaluating colloidal phosphorus delivery to surface waters from diffuse agricultural sources. J. Environ. Qual. 34:287-298.

Hens M., Merckx R. (2001) Functional characterization of colloidal phosphorus species in the soil solution of sandy soils. Environ. Sci. Technol. 35:493-500.

Hens M., Merckx R. (2002) The role of colloidal particles in the speciation and analysis of "dissolved" phosphorus. Water Res. 36:1483-1492.

Hochella M.F., Lower S.K., Maurice P.A., Penn R.L., Sahai N., Sparks D.L., Twining B.S. (2008) Nanominerals, mineral nanoparticles, and Earth systems, Pergamon-Elsevier Science Ltd. pp. A382-A382.

Itami K., Fujitani H. (2005) Charge characteristics and related dispersion/flocculation behavior of soil colloids as the cause of turbidity, Elsevier Science Bv. pp. 55-63.

Kretzschmar R., Borkovec M., Grolimund D., Elimelech M. (1999) Mobile subsurface colloids and their role in contaminant transport, Adv. Agron., Vol 66, Academic Press Inc, San Diego. pp. 121-193.

Kuykendall H.A., Cabrera M.L., Hoveland C.S., McCann M.A., West L.T. (1999) Stocking method effects on nutrient runoff from pastures fertilized with broiler litter. J. Environ. Qual. 28:1886-1890.

Liang L.Y., Mccarthy J.F., Jolley L.W., Mcnabb J.A., Mehlhorn T.L. (1993) Iron dynamics: transformation of Fe(II)/Fe(III) during injection of natural organic-matter in a sandy aquifer. Geochim. Et Cosmochim. Acta 57:1987-1999.

Lin C.Y., Wang Z.G., He M.C., Li Y.X., Liu R.M., Yang Z.F. (2009) Phosphorus sorption and fraction characteristics in the upper, middle and low reach sediments of the Daliao river systems, China. J. Hazard. Mater. 170:278-285.

Makris K.C., Grove J.H., Matocha C.J. (2006) Colloid-mediated vertical phosphorus transport in a waste-amended soil. Geoderma 136:174-183.

Mayer T.D., Jarrell W.M. (1995) Assessing colloidal forms of phosphorus and iron in the tualatin-river basin. J. Environ. Qual. 24:1117-1124.

Maynard J.J., O'Geen A.T., Dahlgren R.A. (2009) Spatial relationships of phosphorus sorption in a seasonally saturated constructed wetland soil. Soil Sci. Soc. Am. J. 73:1741-1753.

Miller A.J., Schuur E.A.G., Chadwick O.A. (2001) Redox control of phosphorus pools in Hawaiian montane forest soils. Geoderma 102:219-237.

Miller N., Quinton J.N., Barberis E., Presta M. (2009) Variability in the mobilization of sediment and phosphorus across 13 European soils. J. Environ. Qual. 38:742-750.

Murphy J., Riley J.P. (1962) A modified single solution method for determination of phosphate in natural waters. Anal. Chim. Acta 26:31.

Nemery J., Garnier J., Morel C. (2005) Phosphorus budget in the Marne Watershed (France): urban vs. diffuse sources, dissolved vs. particulate forms. Biogeochemistry 72:35-66.

Olli G., Darracq A., Destouni G. (2009) Field study of phosphorous transport and retention in drainage reaches. J. Hydrol. 365:46-55.

Pedrot M., Dia A., Davranche M. (2009) Double pH control on humic substance-borne trace elements distribution in soil waters as inferred from ultrafiltration. J. Colloid Interface Sci. 339:390-403.

Pierson S.T., Cabrera M.L., Evanylo G.K., Kuykendall H.A., Hoveland C.S., McCann M.A., West L.T. (2001) Phosphorus and ammonium concentrations in surface runoff from grasslands fertilized with broiler litter. J. Environ. Qual. 30:1784-1789.

Pokrovsky O.S., Schott J. (2002) Iron colloids/organic matter associated transport of major and trace elements in small boreal rivers and their estuaries (NW Russia). Chem. Geol. 190:141-179.

Poppe L.J., Fredericks J.J., Hathaway J.C. (1988) A computer-program to calculate centrifugation parameters for sedimentation analyses. Comput. Geosci. 14:541-545.

Rick A.R., Arai Y. (2011) Role of natural nanoparticles in phosphorus transport processes in ultisols. Soil Sci. Soc. Am. J. 75:335-347.

Ryan J.N., Gschwend P.M. (1990) Colloid mobilization in two Atlantic coastal-plain aquifers: field studies. Water Resour. Res. 26:307-322.

Ryan J.N., Gschwend P.M. (1992) Effect of iron diagenesis on the transport of colloidal clay in an unconfined sand aquifer. Geochim. Cosmochim. Acta 56:1507-1521.

Ryan J.N., Gschwend P.M. (1994) Effect of solution chemistry on clay colloid release from an iron oxide-coated aquifer sand. Environ. Sci. Technol. 28:1717-1726.

Scheidegger A.M., Sparks D.L. (1996) A critical assessment of sorption-desorption mechanisms at the soil mineral/water interface. Soil Sci. 161:813-831.

Sharpley A.N., Kleinman P.J.A., Heathwaite A.L., Gburek W.J., Folmar G.J., Schmidt J.R. (2008) Phosphorus loss from an agricultural watershed as a function of storm size. J. Environ. Qual. 37:362-368.

Sonzogni W.C., Chapra S.C., Armstrong D.E., Logan T.J. (1982) Bioavailability of phosphorus inputs to lakes. J. Environ. Qual. 11:555-563.

Sposito, G. 1992. Characterization of particle surface charge. p. 291-314. *In* Buffle and H.P. van Leeuwen (ed.) Environmental particles. Vol. 1. Lewis Publishers, Chelsea, MI.

Sposito, G. 2000. Ion exchange phenomena. p. B-241-263. *In* M.E. Sumner (ed.) Handbook of soil science. CRC Press, Washington, DC.

Thompson A., Chadwick O.A., Boman S., Chorover J. (2006) Colloid mobilization during soil iron redox oscillations. Environ. Sci. Technol. 40:5743-5749.

Turner B.L., Kay M.A., Westermann D.T. (2004) Colloidal phosphorus in surface runoff and water extracts from semiarid soils of the western United States. J. Environ. Qual. 33:1464-1472.

Verpraskas, M.J., and S.P. Faulkner. 2001. Redox chemistry of hydric soils. p. 85-105. In J.L. Richardson and M.J. Verpraskas (ed.) Wetland soils: Genesis, hydrology, landscapes, and classification. CRC Press, Boca Raton, FL.

Young E.O., Ross D.S. (2001) Phosphate release from seasonally flooded soils: A laboratory microcosm study. J. Environ. Qual. 30:91-101.

APPENDIX A

STOKES-LAW CALCULATION

Particle size fractions will be achieved by subjecting each sample to differential centrifugation. Time (T) for a given particle regime will be calculated assuming ideal spherical geometry according to Equation 2 (Poppe et al., 1988) with the time of acceleration, time of deceleration, fluid viscosity, minimum radius from the rotational axis maximum radius from the rotational axis, particle radius, angular velocity, particle density, and media density.

$$T = \frac{9\eta \ln(R2/R1)}{8\pi^2 N^2 r^2 (\rho - \rho_o)} + \frac{2(ta + td)}{3} \qquad \text{(Equation 2)}$$

Where,
T = time (sec)
ta = time of acceleration (sec)
td = time of deceleration (sec)
η = viscosity (poises)
R1 = minimum radius (cm)
R2 = maximum radius (cm)
r = particle radius (cm)
N = angular velocity (rps)
ρ = particle density (g/cm^3)
ρ_o = media density (g/cm^3)

We assume a fluid viscosity of 0.01003 poises, that particle density is 2.65 g/cm^3 and that the media density is 1.0 g/cm^3. The maximum radius from the rotational axis is 9.5 cm. The minimum radius from the rotational axis is 7 cm.

APPENDIX B

TRANSMISSION ELECTRON MICROGRAPHS AND ENERGY DISPERSIVE X-RAY SPECTROSCOPY ANAYLSIS OF SOIL INCUBATIONS

Micrographs A and B correspond with energy dispersive x-ray spectroscopy analysis C and D respectively unless otherwise stated.

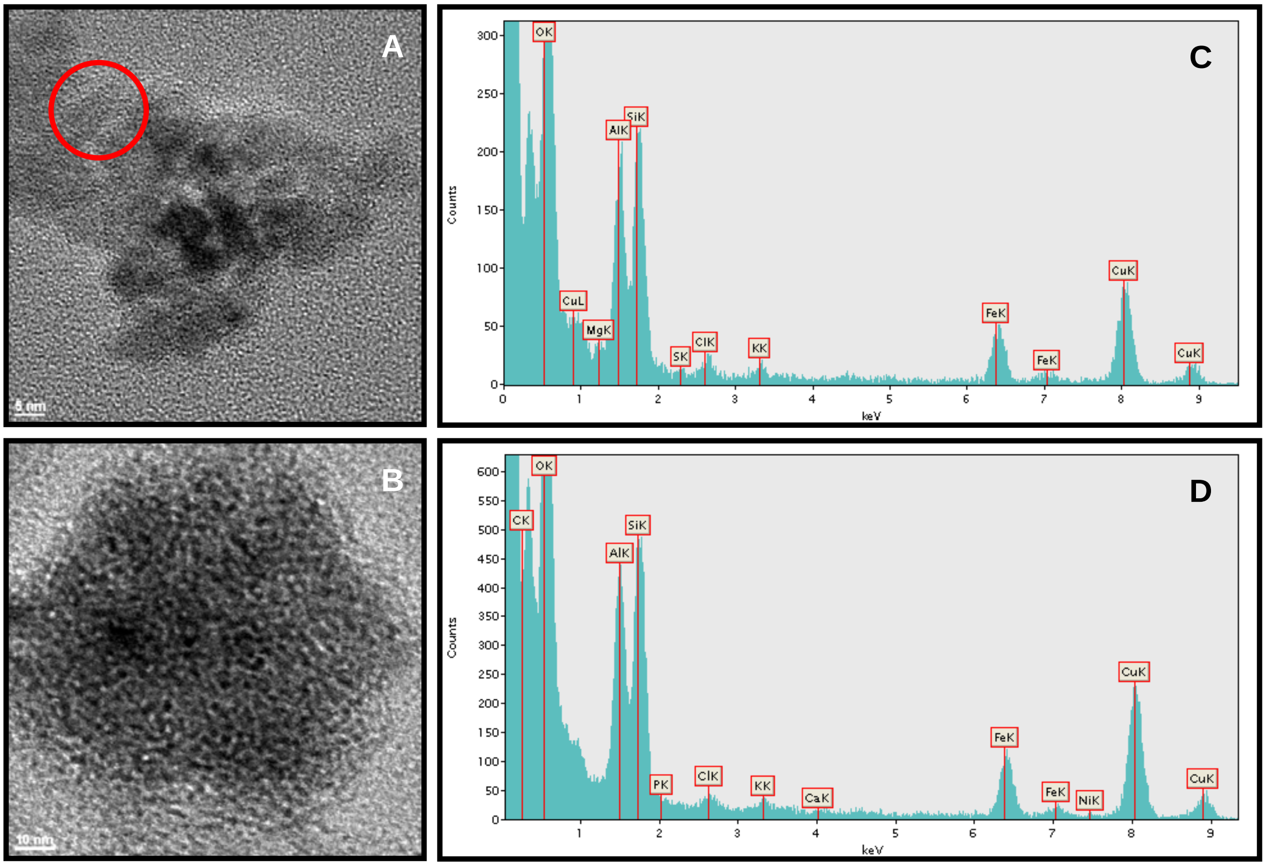

Transmission electron micrographs and corresponding energy dispersive X-ray spectroscopy analysis of Field 2 soil Anoxic incubations spun to remove < 415 nm particles and dialyzed to remove excess salts. Red circle indicates area of micrograph measured by energy dispersive X-ray spectroscopy.

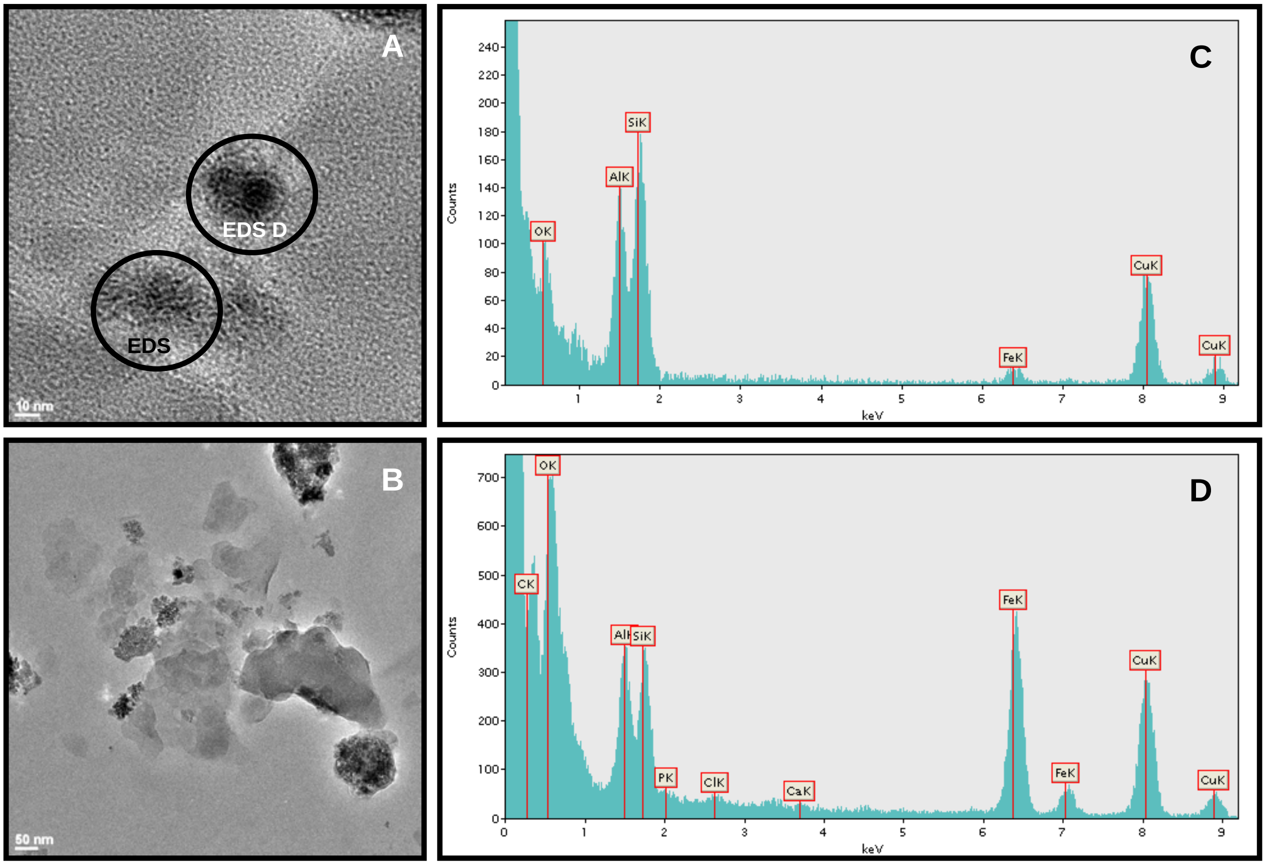

Transmission electron micrographs and energy dispersive X-ray spectroscopy analysis of Field 2 soil Anoxic incubation (A) & Oxic incubation (B) spun to remove < 415 nm particles and dialyzed to remove excess salts.

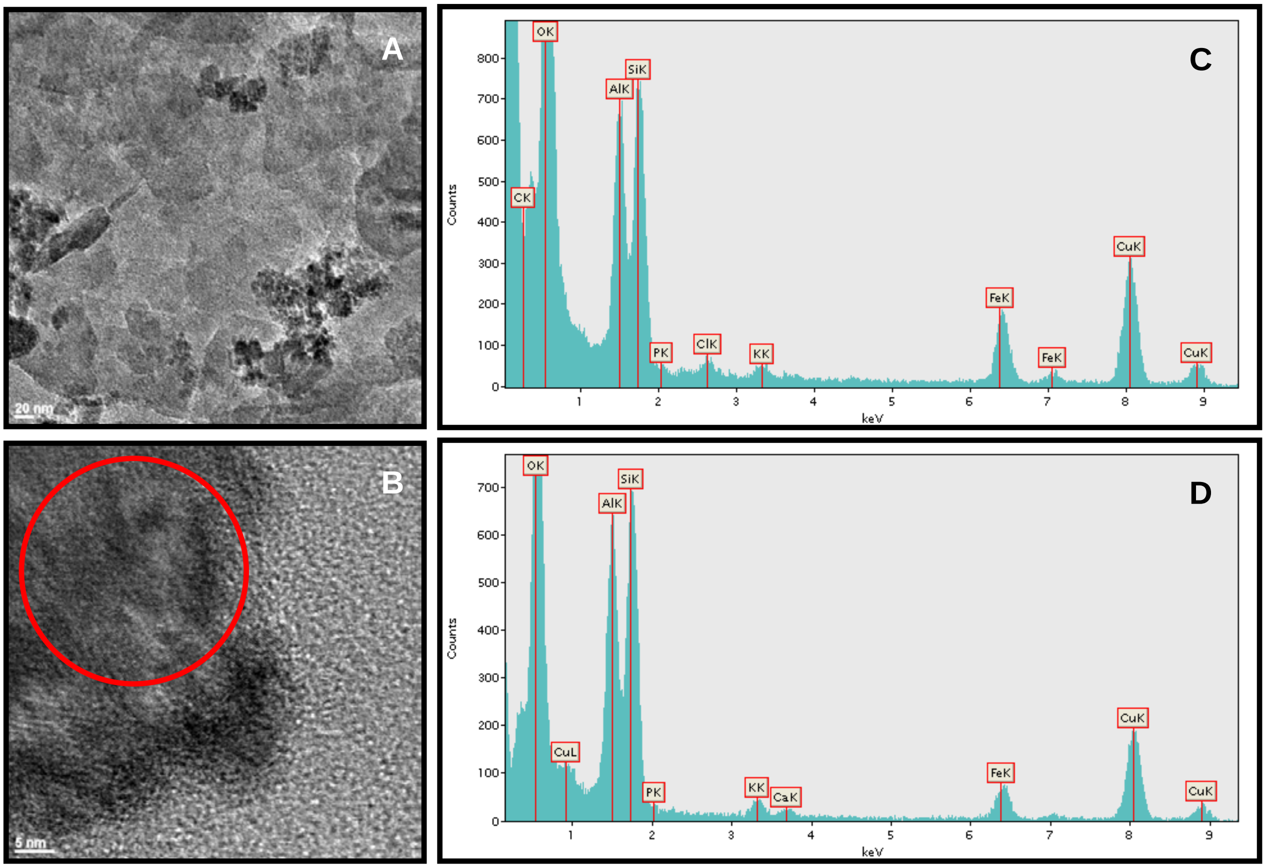

Transmission electron micrographs and energy dispersive X-ray spectroscopy analysis of Field 2 soil Anoxic incubation (A) & Oxic incubation (B) spun to remove < 415 nm particles and dialyzed to remove excess salts. Red circle indicates area of micrograph measured by energy dispersive X-ray spectroscopy.

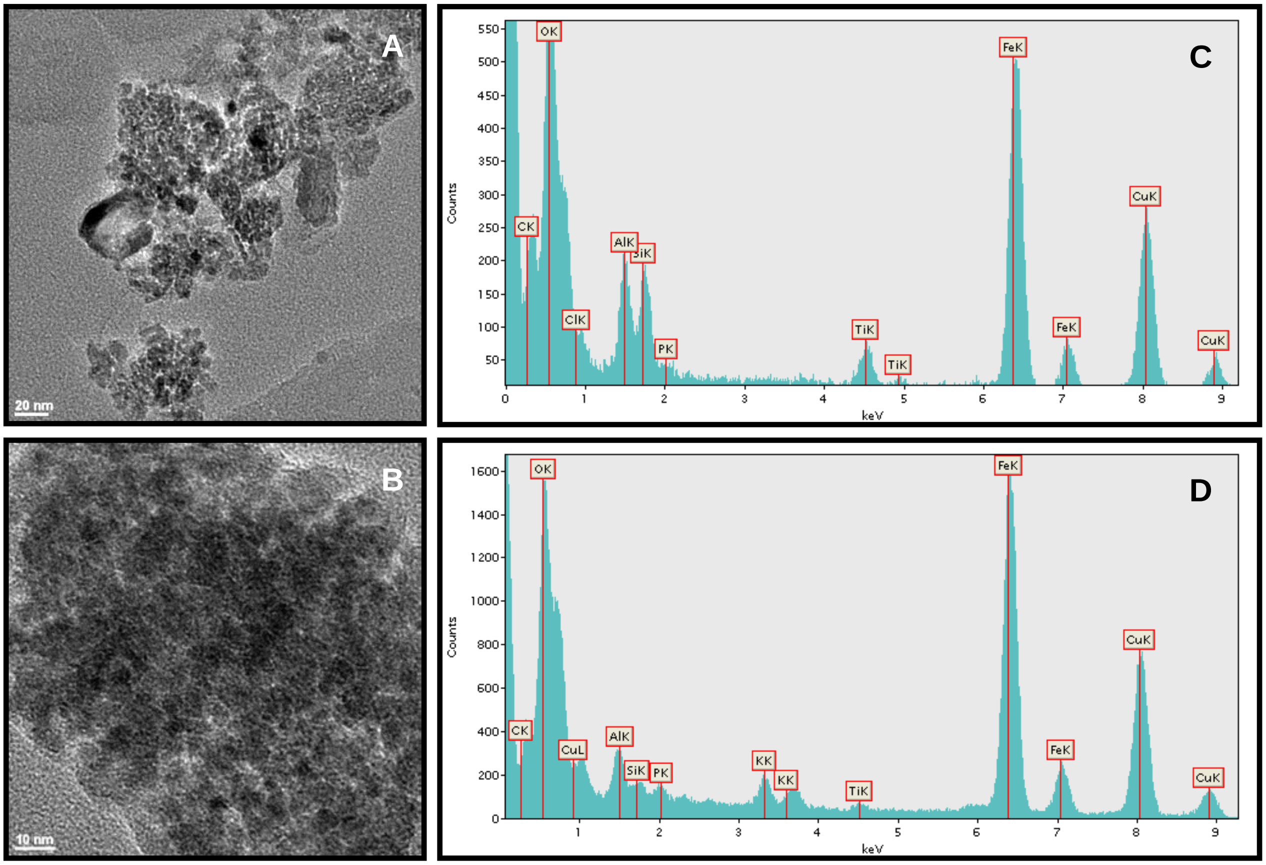

Transmission electron micrographs and corresponding energy dispersive X-ray spectroscopy analysis of Field 2 soil Oxic incubation spun to remove < 415 nm particles and dialyzed to remove excess salts

APPENDIX C

TRANSMISSION ELECTRON MICROGRAPHS AND ENERGY DISPERSIVE X-RAY SPECTROSCOPY ANAYLSIS OF RUNOFF

Micrographs A and B correspond with energy dispersive x-ray spectroscopy analysis C and D respectively.

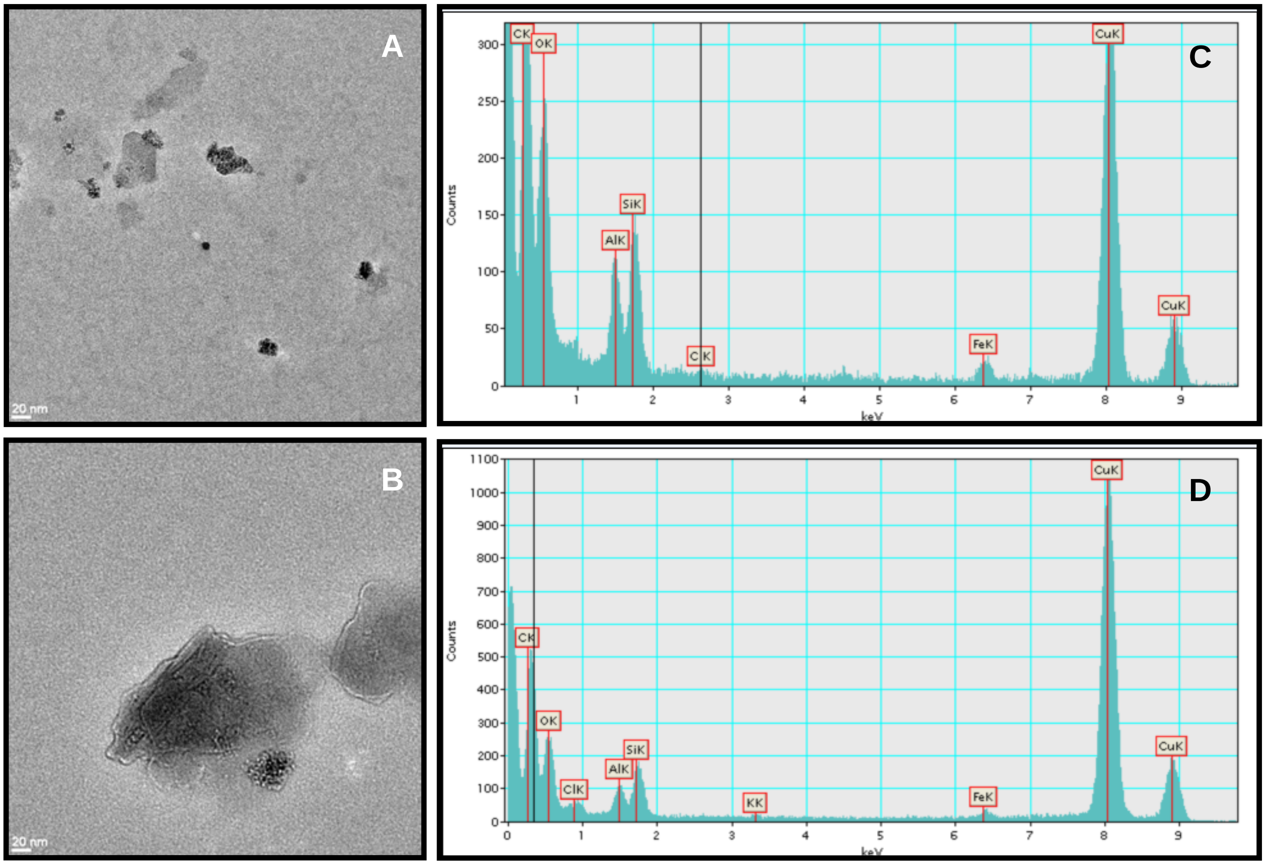

Transmission electron micrographs and corresponding energy dispersive X-ray spectroscopy analysis of runoff.

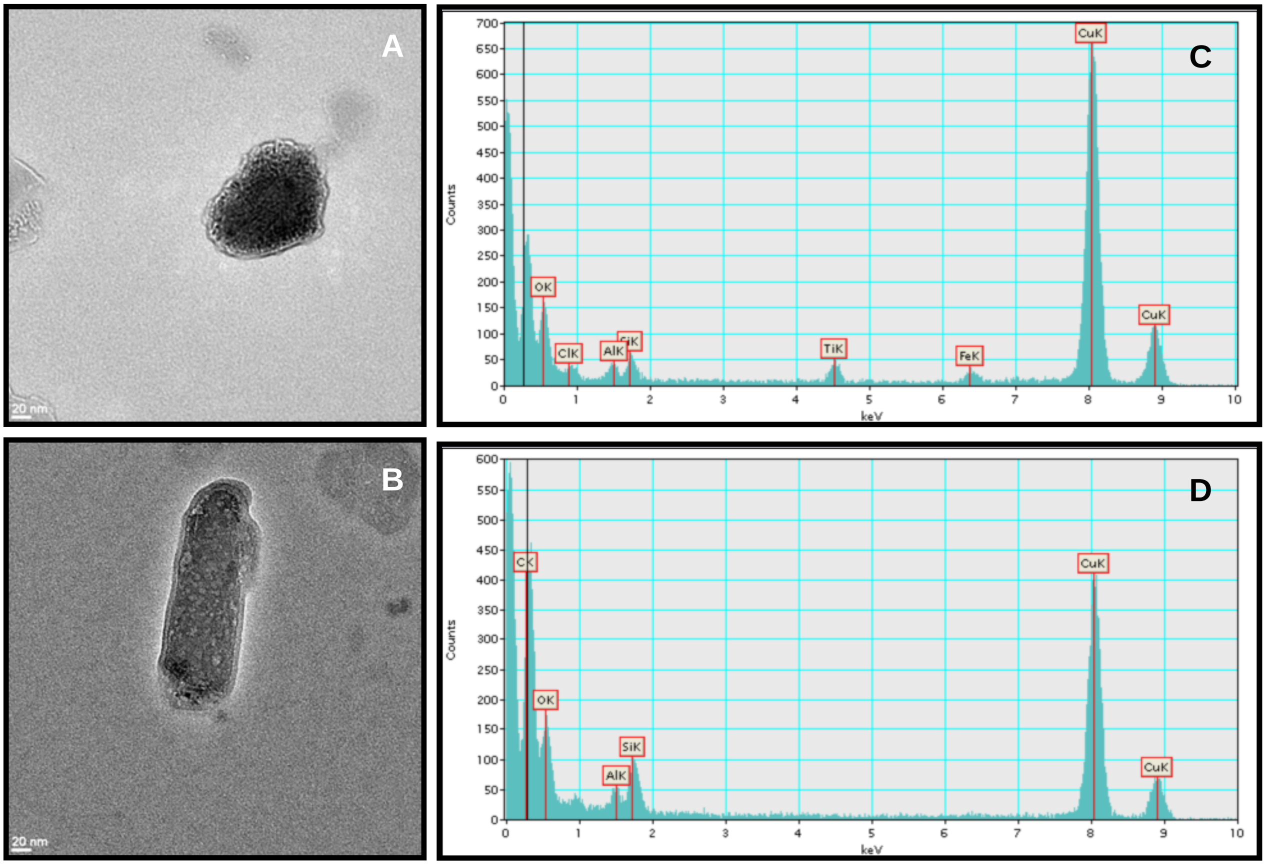

Transmission electron micrographs and corresponding energy dispersive X-ray spectroscopy analysis of runoff.

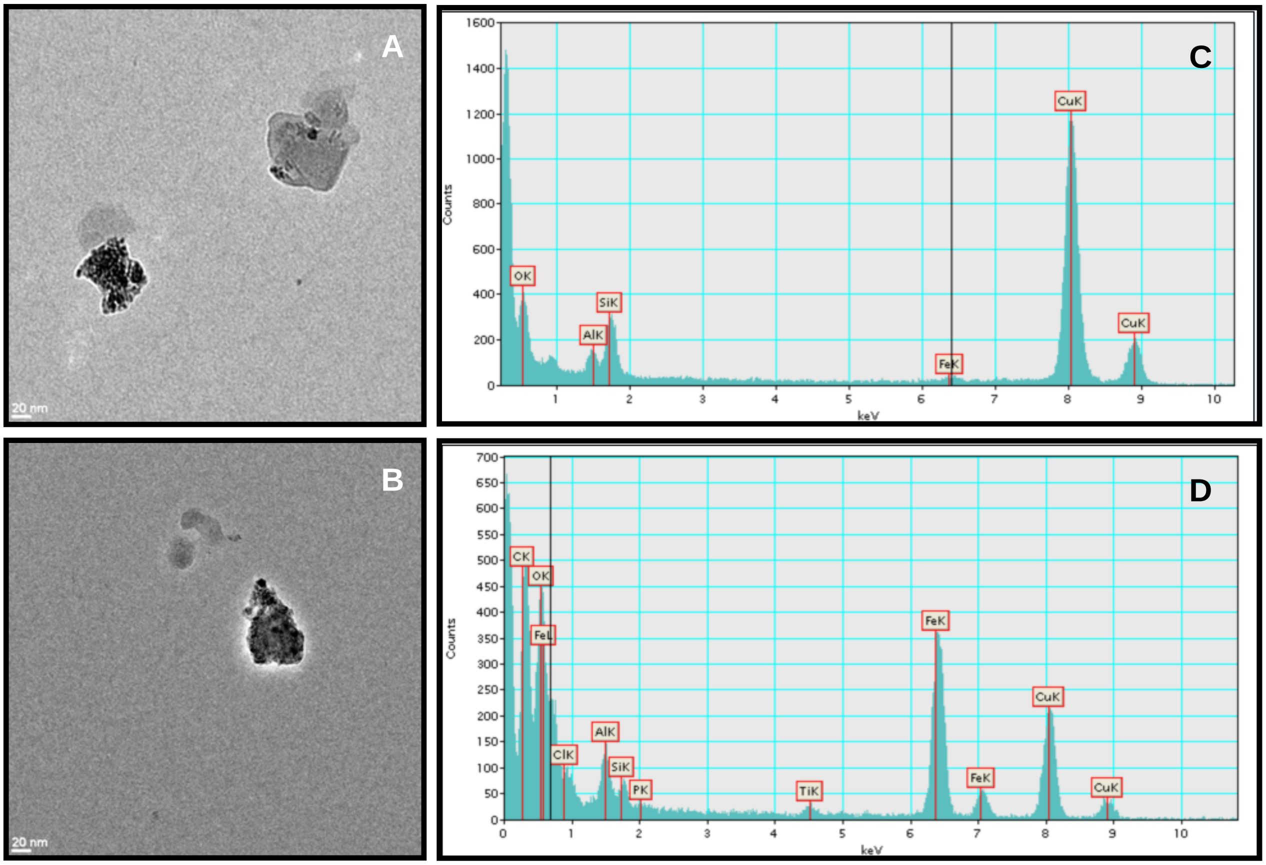

Transmission electron micrographs and corresponding energy dispersive X-ray spectroscopy analysis of runoff.

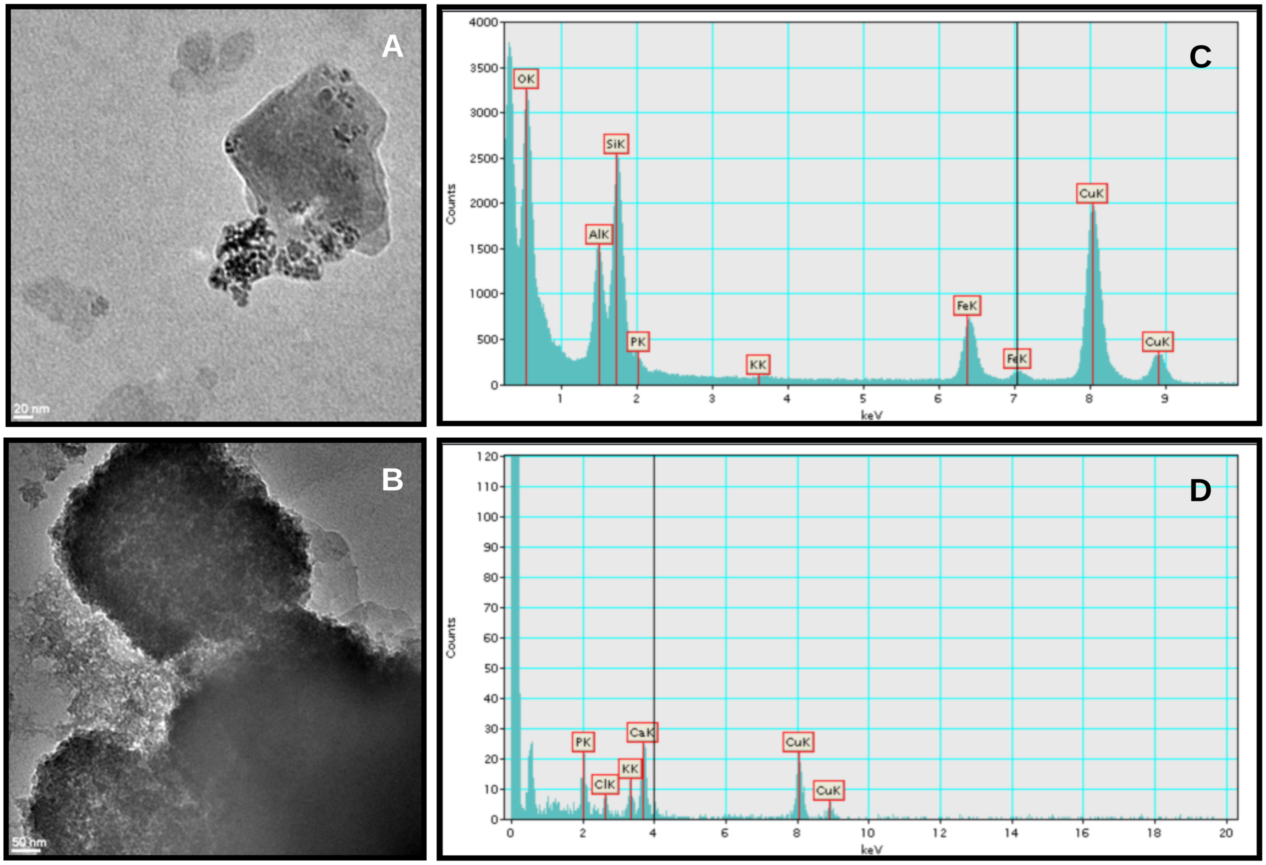

Transmission electron micrographs and corresponding energy dispersive X-ray spectroscopy analysis of runoff.

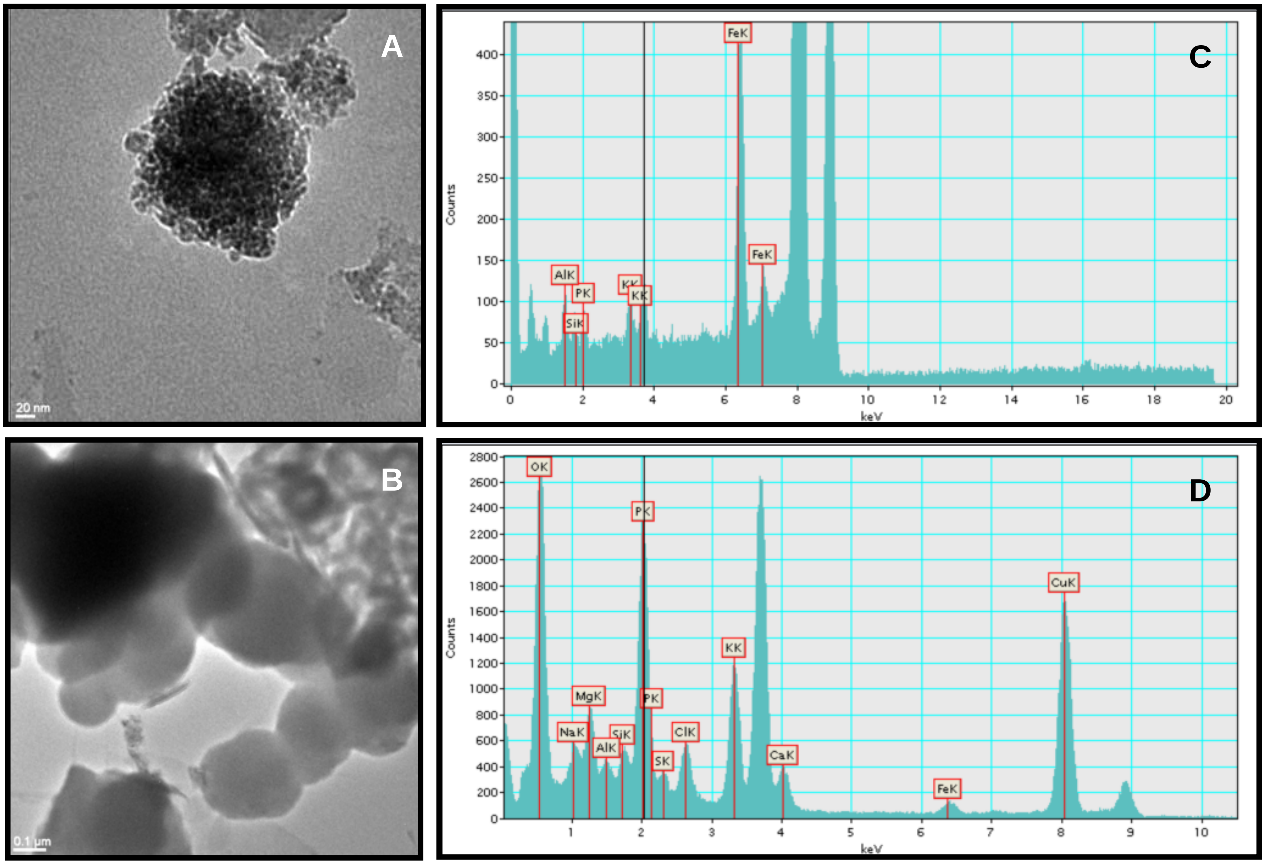

Transmission electron micrographs and corresponding energy dispersive X-ray spectroscopy analysis of runoff.

APPENDIX D

SOIL CHARACTERIZATION DATA

	Microwave Digestion						P Fractionation			
	P	Fe	Al	Ti	Si	Ca	H_2O	$NaHCO_3$	NaOH	HCl
Field	mmol kg^{-1}						mmol P kg^{-1}			
1	15.8	112.1	627.2	15.8	733.0	89.1	2.43	7.57	14.62	1.92
2	15.2	122.0	531.7	31.0	716.4	102.8	2.64	9.02	18.88	2.22
3	22.0	128.8	498.9	26.6	760.6	107.3	2.10	8.08	17.43	3.51
6	17.2	252.7	331.1	10.5	825.3	141.0	0.93	6.98	18.56	2.14
7	5.8	101.9	569.6	22.1	818.2	66.6	0	0.47	3.05	0.24
9	5.7	103.0	308.6	13.9	892.9	159.2	0	0.47	4.93	0.70